Optical characterization of tissue
for medical diagnostics

Charlotta Eker

OPTICAL CHARACTERIZATION OF TISSUE FOR MEDICAL DIAGNOSTICS

Charlotta Eker

Till Johan

Contents

Abstract

This thesis deals with the development and evaluation of some different optical techniques for tissue characterization. The main aim has been to improve and evaluate such investigative techniques in *in vivo* studies. In this attempt a key issue has been to gain understanding in the underlying mechanisms of laser-based diagnostics of premalignant and malignant lesions and to evaluate methods for efficient analysis of acquired data. In particular, photon migration-based methods, aiming at the characterization of thick tissues such as the female breast, and laser-induced fluorescence for detection of superficial malignant and premalignant lesions have been studied.

Novel time and frequency domain techniques have been employed to determine the optical properties at multiple wavelengths in healthy breast tissue of volunteers. These techniques have proven to be capable of simultaneously determining the fat, water and haemoglobin concentrations in the tissue. This might be essential in the effort to find a reliable intrinsic contrast for optical breast cancer detection. Another technique, based on interference between photon density waves, is improved and its potential for detection of small inhomogeneities in turbid media is evaluated.

The potential of laser-induced fluorescence (LIF) spectroscopy to distinguish between malignant, premalignant and benign lesions *in vivo* in the colon and in the larynx has been studied. This is an interesting technique, since it could provide information about tissue pathology in real-time during endoscopic examination, thus reducing sampling error in the biopsy procedure. LIF could also help the physician characterize and demarcate lesions for optimal therapy. The technique is shown to be a powerful tool during colonoscopy – fluorescence could to a high degree of accuracy distinguish neoplastic polyps from non-neoplastic polyps and normal mucosa. Also the results from the larynx are promising, lesions could be distinguished from normal, and different lesion types could to some degree be separated. Both autofluorescence and the characteristic fluorescence from δ-aminolevulinic acid induced protoporphyrin IX have been studied. Different statistical tools for evaluation of fluorescence emission spectra have been used. In particular, multivariate analysis tools such as multivariate linear regression and partial least squares analysis have been employed. Fluorescence imaging of basal cell carcinomas on the skin, using a multi-wavelength and a fluorescence lifetime system has been performed.

List of papers

This thesis is based on the following papers:

I.   C. af Klinteberg, C. Eker, A. Pifferi, O. Jarlman, S. Svanberg and S. Andersson-Engels, Time- and wavelength resolved spectroscopy of female breast tissue, Manuscript in preparation (1999).

II.   C. Lindquist, A. Pifferi, R. Berg, S. Andersson-Engels and S. Svanberg, Reconstruction of diffuse photon-density wave interference in turbid media from time-resolved transmittance measurements, *Appl. Phys. Lett.* **69**, 1674-1676 (1996). (∗)

III.   C. Lindquist, A. Pifferi, S. Andersson-Engels and S. Svanberg, Reconstruction of diffuse photon density wave interference for detection of small inhomogeneities in turbid media, in Advances in Optical Imaging and Photon Migration, eds. R.R. Alfano and J.G. Fujimoto, OSA Trends in Optics and Photonics **2**, 148-151 (1996). (∗)

IV.   C. Eker, N. Shah, T. Pham and B. Tromberg, Non-invasive determination of blood, water, and fat content in human breast tissue using frequency-domain photon migration spectroscopy, Manuscript for *Photochem. Photobiol.* (1999).

V.   N. Shah, C. Eker, J. Espinoza, J. Fishkin, R. Hornung, B. Tromberg and J. Butler, Multi-wavelength, *in vivo* measurements of human breast tissue optical properties reveal hormonal-dependent absorption and scattering variations, Manuscript for *Proc. Natl. Acad. Sci.* (1999).

VI.   C. Eker, S. Montán, E. Jaramillo, K. Koizumi, C. Rubio, S. Andersson-Engels, K. Svanberg, S. Svanberg and P. Slezak, Clinical spectral characterisation of colonic mucosal lesions using autofluorescence and δ-aminolevulinic acid sensitisation, *Gut* **44***, 511-518* (1999).

VII.   C. Eker, E. Jaramillo, S. Andersson-Engels, E. Jonas, C. Rubio, P. Slezak and K. Svanberg, Colonic epithelial polyp discrimination *in vivo* using laser-induced fluorescence, Submitted to *Gastroenterology* (1999).

VIII. R. Rydell, C. Eker, S. Andersson-Engels, P. Wahlberg and K. Svanberg, Fluorescence investigations to classify malignant laryngeal lesions *in vivo*, Manuscript for *Head and Neck* (1999).

IX.   C. Eker, R. Rydell, K. Svanberg and S. Andersson-Engels, Multivariate analysis of laryngeal fluorescence spectra recorded *in vivo*, Submitted to *Lasers Surg. Med.* (1999).

X.   S. Andersson-Engels, G. Canti, R. Cubeddu, C. Eker, C. af Klinteberg, A. Pifferi, K. Svanberg, S. Svanberg, P. Taroni, G. Valentini and I. Wang, Preliminary evaluation of two fluorescence imaging methods for detection of basal cell carcinomas of the skin, *Lasers Surg. Med.,* In press (1999).

Additional material is presented in

C. Lindquist, R. Berg and S. Andersson-Engels, Numerical diffusion modelling of interfering photon density waves for optical mammography, in *Photon Transport in Highly Scattering Tissue*, eds. S. Avrillier, B. Chance, G.J. Müller, A.V. Priezzhev and V.V. Tuchin, Proc. SPIE **2326**, 31-40 (1994). (∗)

C. af Klinteberg, R. Berg, C. Lindquist, S. Andersson-Engels and S. Svanberg, Diffusely scattered femtosecond white light examination of breast tissue *in vitro* and *in vivo*, in *Photon Propagation in Tissues*, eds. B. Chance, D.T. Delpy and G.J. Müller, Proc. SPIE **2626**, 149-157 (1995). (∗)

C. af Klinteberg, C. Lindquist, A. Pifferi, R. Berg, S. Andersson-Engels and S. Svanberg, Diffusely scattered femtosecond white light examination of breast tissue, in *Medical and Biological Applications*, ed. R. Cubeddu, Proc. OSA Trends in Optics and Photonics **6**, 30-35 (1996). Invited paper. (∗)

C. af Klinteberg, C. Lindquist, I. Wang-Nordman, A. Vaitkuviene and K. Svanberg, Laser-induced fluorescence studies of premalignant and benign lesions in the female genital tract, in *Optical Biopsies and Microscopic Techniques II*, eds. I.J. Bigio, K. Svanberg, H. Schneckenburger, J. Slavik and P.M. Viallet, Proc. SPIE **3197**, 34-40 (1997). (∗)

R. Cubeddu, A. Pifferi, P. Taroni, G. Valentini, G. Canti, C. Lindquist, S. Andersson-Engels, S. Svanberg, I. Wang and K. Svanberg, Multispectral and lifetime imaging for the detection of skin tumors, in *Biomedical Optical Spectroscopy and Diagnostics/Therapeutic Laser Applications*, eds. E.M. Sevick-Muraca, J.A. Izatt and M.N. Ediger, Proc. OSA Trends in Optics and Photonics **22**, 106-109 (1998). (∗)

(∗) Please note that the author published some of the papers under her maiden name, Lindquist.

Nomenclature

SYMBOL	DESCRIPTION	DEFINITION	UNIT
a'	reduced albedo	$a'=\mu_s'/(\mu_a+\mu_s')$	
c	speed of light in medium	$c=c_0/n$	m·s^{-1}
c_0	speed of light in vacuum		m·s^{-1}
C	concentration		mol·m^{-3}
D	diffusion coefficient	$D=(3\mu_{tr})^{-1}$	m
f	frequency		s^{-1}
$\mathbf{F}(\mathbf{r},t)$	photon flux	$\mathbf{F}(\mathbf{r},t) = \int\limits_{4\pi} L(\mathbf{r},\mathbf{s},t)\mathbf{s}d\Omega$	W·m^{-2}
g	anisotropy factor, average cosine of scattering angle	$g = \int\limits_{4\pi} \cos\theta \cdot p(\cos\theta)d\Omega$	
k	wave number		m^{-1}
$L(\mathbf{r},\mathbf{s},t)$	radiance		W·m^{-2}·sr^{-1}
$<L>$	average path length		m
M	modulation		
n	refractive index		
N($\mathbf{r},\mathbf{s},t$)	number of photons per unit volume and unit angle		m^{-3}·sr^{-1}
$p(\mathbf{s},\mathbf{s'})$	phase function		
$Q(\mathbf{r},\mathbf{s},t)$	source term		W·m^{-3}·sr^{-1}
$\mathbf{r}$	position		
$R(\rho,t)$	diffuse reflectance, backscattering		W·m^{-2}
R_{eff}	effective reflection coefficient	see Haskell *et al* [1]	
$\mathbf{s},\mathbf{s'}$	unit vectors		
$S(\mathbf{r},t)$	source term		W·m^{-3}
t	time		s
T(ρ,t)	diffuse transmittance		W·m^{-2}
z_0	mean free path of isotropic scattering	$z_0=(\mu_s')^{-1}$	m
ε	extinction coefficient		m^2·mol^{-1}
$\varphi(\mathbf{r},t)$	fluence rate		W·m^{-2}
ϕ	phase angle		rad
λ	wavelength		m
μ_a	absorption coefficient		m^{-1}
μ_{eff}	effective attenuation		
μ_s	scattering coefficient		m^{-1}
μ_s'	reduced scattering coefficient	$\mu_s'=\mu_s(1-g)$	m^{-1}
μ_{tr}	transport coefficient	$\mu_{tr}=\mu_a+\mu_s'$	m^{-1}
Ω	solid angle		sr
ρ	distance		m
θ	(scattering) angle		rad
ω	angular frequency	$\omega=2\pi f$	rad·s^{-1}

Abbreviations and acronyms

AC	alternating current	23
ALA	δ-aminolevulinic acid	58
CCD	charge-coupled device	60
CIS	carcinoma *in situ*	51
DC	direct current	23
DPDW	diffuse photon density wave	*25*
EEM	excitation–emission matrix	53
FAD	flavin adenine dinucleotide	54
FDPM	frequency domain photon migration	*42*
Hb	deoxygenated haemoglobin	29
HbO$_2$	oxygenated haemoglobin	29
HpD	haematoporphyrin derivative	58
IR	infrared	28
LIF	laser-induced fluorescence	15, *47*
MVLR	multivariate linear regression	66, *70*
NAD$^+$	oxidized nicotinamide adenine dinucleotide	55
NADH	the reduced form of NAD$^+$	15, *55*
NIR	near-infrared	30
OMA	optical channel analyser	60
PCA	principal component analysis	66, *71*
PCR	principal component regression	66
PDT	photodynamic therapy	58, *63*
PLS	partial least squares	66, *72*
PpIX	protoporphyrin IX	58
UV	ultraviolet	28

Chapter 1
Introduction

Light has been used both for detection and therapy of cancer since the beginning of the century.[2-4] Almost as soon as the first laser was operated by Maiman in 1960, the new possibilities for its application in medicine were recognized. The possibility to choose a laser source with a particular wavelength to target some specific type of molecule, often water or haemoglobin, is very valuable. The light intensity and duration can also be varied to achieve certain effects. The use of light to identify malignancy is an appealing approach in many clinical specialties, since molecular changes can be detected, and not only tissue morphology as in most conventional techniques. In this thesis some optical methods for the characterization of biological tissues, in particular of malignant and premalignant lesions, are studied and evaluated. Two types of techniques are considered: photon migration based measurements, mainly aiming at detecting and characterizing lesions in the female breast, and fluorescence measurements, which identify superficial tissue lesions. The use of optical fibres enables fluorescence measurements during endoscopic examinations inside hollow organs of the body. All techniques presented in this thesis use light at sufficiently low intensities and long wavelengths to be harmless to the tissue.

The thesis consists of an introduction and ten original scientific papers. The introduction describes some of the theories used and gives a background to the papers, since these often focus more on the new findings than on the theoretical framework. The data presented in the papers were collected in physics laboratory environments at the Lund Institute of Technology and at the University of California, Irvine, as well as in clinical settings at the Lund University Hospital and the Karolinska Hospital in Stockholm.

The work described in this thesis has mainly been of applied nature, focusing on the analysis of measured data. However, the theory of light absorption and scattering in tissues is the basis for all work within the biomedical optics field, and is

therefore outlined in Chapter 2. Transport of near-infrared light used in this work can in most tissues be described as a diffusion process. The optical properties of tissue, i.e. the scattering and absorption, vary depending on light wavelength, tissue type and status. Variations in optical properties can hence be used for tissue diagnostics, e.g. as an indication of tumour tissue or internal bleeding. The optical properties can be measured noninvasively by different techniques, and some of these are described in Chapter 3. Specifically, the time- and frequency-resolved methods used in Papers I-V are described. These methods have been used to determine the optical properties of female breast tissue, by sending in light through the skin. In the work of this thesis, mainly healthy breast tissue has been examined, in order to study what variations in optical properties can be expected between individuals and depending on age, hormonal status, etc. There are also indications that the breast optical properties will vary depending on the pathological state of the tissue.[5,6] If the variations due to malignant transformation are found to be larger than the normal variations, optical techniques could prove to be valuable complements to x-ray based mammography examinations. Although optical methods have the potential of extracting information not available with other currently used diagnostic methods, they also have some limitations for detecting deeply located tumours. Firstly, light is heavily attenuated and only weak signals are available. Secondly, the main attenuation is caused by scattering, meaning that all detected light will be diffuse, and the spatial resolution will be very poor. These aspects are discussed in Chapter 2.

As early as 1929, Cutler performed optical transillumination of female breast tissue for the purpose of detecting tumours.[2] He sent visible light from a lamp through the breast of a patient sitting in a totally dark room. The transmitted light was examined directly by the eye. He observed that solid tumours often were opaque to the light. However, malignant lesions could not be distinguished from benign lesions. Later studies were performed with continuous light sources and video detection,[7] but the results from different studies were conflicting. However, research in the area was pursued, since the conventional method for breast screening, x-ray mammography, has its limitations in that potentially harmful ionising radiation is used. X-ray mammography has also some other weak points. It does not have a very high sensitivity for certain breast tumour types, for example the aggressive necrotic comedo cancers, and it has limited sensitivity for tumour detection in x-ray dense breast tissue of younger women. The issue of screening is a constant source of controversy in the research community, at least concerning women under 50 years of age.[8] Optical methods might offer an alternative for young women, especially for those who have increased sensitivity to ionizing radiation or who have hereditary breast cancer in the family.[9] They could also be used as complements to conventional mammography. Optical methods cannot yield a spatial resolution comparable to that obtained by x-ray mammography or ultrasound, but they can provide additional sensitivity and specificity to the diagnostic procedure by

indirectly measuring physiological information not measurable by other techniques. By making measurements at several wavelengths, physiological properties of the tissue, such as blood volume, haemoglobin oxygenation and fat and water concentrations in the tissue can be determined (Papers IV and V).

The other main subject studied in this thesis is fluorescence spectroscopy of tissues. Fluorescence techniques usually measure only the most superficial cell layers in the tissue, as opposed to the techniques for breast measurements presented above, which can probe several centimetres into the tissue. Different biomolecules in tissue emit fluorescence when illuminated with blue or ultraviolet light. The measured fluorescence signal depends on the concentration of these molecules, but also on tissue optical properties, i.e. on microscopic and macroscopic tissue architecture.[10-12] The aim is a noninvasive measurement technique, which is able to characterize tissue in real-time during an examination. The use of lasers as light sources offers the possibility of efficiently guiding the light through optical fibres. The fibres can be inserted through endoscopic instruments, enabling fluorescence measurements inside most hollow organs of the body.

In 1911, one of the first studies of fluorescence from tissue was performed[13]. In 1924, it was noted that endogenous porphyrins could be responsible for red fluorescence from animal tumours[3]. The major substances responsible for the fluorescence from tissue at near-ultraviolet excitation were later identified as collagen, elastin, tryptophan, flavins and reduced nicotinamide adenine dinucleotide (NADH)[14-16]. Laser-induced fluorescence (LIF) studies employ either the differences in UV-induced intrinsic fluorescence (autofluorescence) from tissue in different pathological states,[17-19] or the fluorescence following administration of a fluorescent tumour marker.[20-23] The present gold standard for diagnosis is based on histopathological methods, where tissue samples are collected, thoroughly prepared and analysed under a microscope.

The search for a complementary method that could discriminate between lesion types and find the margins of lesions in real-time is clinically highly relevant. Fluorescence techniques are described in Chapter 4, giving a medical and physical background to Papers VI to X. Clinical measurements made in the colon and on the vocal folds, looking at autofluorescence or using a fluorescent tumour marker, are reported in Papers VI to IX. Two fluorescence imaging techniques have been used for measurements on skin lesions in Paper X. Different evaluation techniques have been employed in these studies. Paper IX reviews different multivariate analysis methods available for the evaluation of fluorescence spectra. The background to these multivariate data analysis methods and some other possible spectral analysis tools is given in Chapter 5.

Chapter 2
Light transport in tissue

If light is sent into biological tissue, different processes can occur. While most of the light enters the tissue, a small part of it can be reflected off the tissue surface. The amount of reflected light depends on the angle of incidence and the index of refraction. Inside the tissue, the light can be absorbed or scattered. Both processes are highly wavelength dependent. In the lower part of the visible wavelength region, the scattering probability is comparable to the absorption. In the red and near-infrared wavelength region light penetrates tissue better. This region is called the optical window. In this wavelength range the absorption is low and scattering dominates. Most diagnostic applications use light in this wavelength region. Based on measurements of optical properties, physiological or structural information about the probed tissue can be extracted. This chapter will outline the mathematical basis of light transport in tissues and describe the tissue features that affect this transport.

2.1   Light transport theory

The process of light transport in turbid media may be described mathematically either by analytical theory, based directly on Maxwell's equations, or by transport theory. Maxwell's equations can describe the interaction between light and tissue as an electromagnetic wave propagating through a medium with random dielectric fluctuations. However, due to the complex structure of tissue it is in principle impossible to obtain a formulation that takes all its dielectric properties into account.[24]

Transport theory, on the other hand, treats the problem as a flow of power through a scattering medium. Transport theory is less mathematically rigorous than electromagnetic theory and does not in itself include effects such as diffraction or interference. However, it has proven useful for calculating photon transport in tissue. It is usually expressed for the radiance $L(\mathbf{r},\mathbf{s},t)$ [Wm^{-2}sr^{-1}], which is the radiant power per unit area and unit solid angle in direction $\mathbf{s}$, at a position in space $\mathbf{r}$. It is

obtained by multiplying the light distribution function, $N(\mathbf{r},\mathbf{s},t)$ [m⁻³sr⁻¹], with the speed and energy of the photons in the medium. Radiance is the quantity used to describe the propagation of photon power. The transport equation can be formulated as

$$\frac{1}{c}\frac{\partial L(\mathbf{r},\mathbf{s},t)}{\partial t} = -\mathbf{s}\cdot\nabla L(\mathbf{r},\mathbf{s},t) - \left(\mu_s + \mu_a\right)L(\mathbf{r},\mathbf{s},t) +$$
$$+ \mu_s\iint\limits_{4\pi} L(\mathbf{r},\mathbf{s}',t)p\left(\mathbf{s},\mathbf{s}'\right)d\Omega' + Q\left(\mathbf{r},\mathbf{s},t\right), \tag{1}$$

where c is the speed of light in the tissue, $c=c_0/n$ where c_0 is the speed of light in vacuum and n is the refractive index of the medium. The scattering and absorption coefficients μ_s and μ_a describe the probability of a scattering or absorption event per unit length. The phase function, $p(\mathbf{s},\mathbf{s}')$ denotes the probability that a scattered photon initially travelling in direction $\mathbf{s}'$ continues in direction $\mathbf{s}$ after the scattering event. The integral of the probability density function over all solid angles $d\Omega'$ is equal to one. The transport equation describes the energy balance in an infinitesimal volume element in the tissue. The left-hand side of Equation (1) is the change in number of photons at position $\mathbf{r}$, with direction $\mathbf{s}$ at time t. On the right-hand side, the first two terms describe the loss of photons, due to escape over the volume boundaries, scattering into other directions or absorption. The third term represents the gain through photons that are scattered from other directions into direction $\mathbf{s}$, while the last term is gain due to a light source. It is assumed that all photons have the same energy and that all scattering is elastic.

It is further assumed that the scattering is symmetric about the incident wave, which means that the phase function is a function of the scattering angle alone, such that $p(\mathbf{s},\mathbf{s}')=p(\theta)$, where θ is the angle between the incident and the scattered photon. It is often useful to have an analytic expression for the phase function. The most popular phase function for light transport in biological tissue is the Henyey-Greenstein function[25]

$$p\left(\mathbf{s},\mathbf{s}'\right) = p\left(\cos\theta\right) = \frac{\left(1-g^2\right)}{4\pi\left(1+g^2-2g\cos\theta\right)^{3/2}}, \tag{2}$$

where g, the anisotropy factor, is the mean cosine of the scattering angle θ. For nearly isotropic scattering, the value of g is close to zero, while a g close to unity indicates a strongly forward directed scattering. Tissue is in general highly forward scattering.

Analytic solutions to the transport equation are only known for a few special cases[26]. In practise, either numerical methods such as Monte Carlo simulations or expansion in spherical harmonics, leading after truncation to the diffusion equation discussed in chapter 2.2, are used. The Monte Carlo method simulates a migration of photon packages in a scattering and absorbing medium. The simulated interaction events of these photon packages are based on random samplings from probability distributions of the step size between interaction events and scattering angles. For each scattering event, the light is also attenuated due to absorption. The trajectory of the photon package is followed until it exits through a boundary or is totally lost by absorption. The Monte Carlo method is useful in that it can be used for any geometry, including layered and inhomogeneous media, and for any optical properties. The main disadvantage is that, due to the statistical nature of the method, a large number of photon packages have to be simulated, requiring long computation times.

2.2 Diffusion

One way of solving the transport equation analytically is to simplify the problem further using an expansion method. The radiance $L(\mathbf{r},\mathbf{s},t)$, the phase function $p(\mathbf{s},\mathbf{s}')$ and the source function $Q(\mathbf{r},\mathbf{s},t)$ are then expanded in spherical harmonics. The lowest order (P_1) approximation is a truncation of the series expansion and includes just the zeroth and first terms in the infinite series. The radiance can then be expressed as

$$L \approx \frac{1}{4\pi}\varphi(\mathbf{r},t) + \frac{3}{4\pi}\mathbf{F}(\mathbf{r},t)\cdot\mathbf{s},\qquad(3)$$

where $\varphi(\mathbf{r},t)$ [Wm^{-2}] is the fluence rate and $\mathbf{F}(\mathbf{r},t)$ [Wm^{-2}] is the photon flux. The fluence rate is defined as the radiant power incident on a small sphere divided by the cross-sectional area of that sphere

$$\varphi(\mathbf{r},t) = \int_{4\pi} L(\mathbf{r},\mathbf{s},t)d\Omega.\qquad(4)$$

In a totally isotropic light field, $L=\varphi/4\pi$, corresponding to the first term on the right hand side of Equation (3). The flux describes photon energy transfer per unit area

$$\mathbf{F}(\mathbf{r},t) = \int_{4\pi} L(\mathbf{r},\mathbf{s},t)\mathbf{s}d\Omega.\qquad(5)$$

The P$_1$ approximation is only valid if the higher order terms in the series expansion are negligible. The radiance is then approximated to an isotropic term (φ) plus a perturbation (**F**). The flux can be related to the fluence rate through Fick's law

$$\mathbf{F} = -D\nabla\varphi, \tag{6}$$

which states that the photon flux is proportional to the gradient of the fluence rate. The proportionality factor D is called the diffusion coefficient, given by

$$D = \left(3\mu_{tr}\right)^{-1} = \left(3\left(\mu_a + \mu_s{'}\right)\right)^{-1} \tag{7}$$

where $\mu_s{'}$, called the reduced scattering coefficient, is given by $\mu_s{'}=\mu_s(1-g)$. This is in principle the result of a transform from nonisotropic to isotropic conditions, yielding a coefficient for the effective isotropic scattering. The reduced scattering $\mu_s{'}$ is smaller than μ_s, indicating that a number ($(1-g)^{-1}$) of nonisotropic scattering events can effectively be seen as one single isotropic scattering event. The transport coefficient μ_{tr} corresponds to the inverse of the effective mean free path, i.e. the mean distance travelled by a photon between interactions (absorption or effective isotropic scattering). If we insert the spherical harmonics of the radiance, phase function and source function into Equation (1) and use Fick's law, this yields the diffusion equation

$$\frac{1}{c}\frac{\partial}{\partial t}\varphi\left(\mathbf{r},t\right) - D\nabla^2\varphi\left(\mathbf{r},t\right) + \mu_a\varphi\left(\mathbf{r},t\right) = S\left(\mathbf{r},t\right), \tag{8}$$

where $S(\mathbf{r},t)$ is a source term. A homogeneous tissue, hence a constant diffusion coefficient, has been assumed. The diffusion approximation implies a substitution of the radiance with an isotropic distribution and a small directional perturbation, and is only valid if the light distribution can be considered as diffuse. The requirements are thus that the reduced scattering coefficient must be much larger than the absorption, i.e. $\mu_s{'} \gg \mu_a$, and that the point **r**, where we are looking, is far from sources and boundaries. The first requirement is true for most tissues in the red and near-infrared wavelength region. The diffusion coefficient D as defined in Equation (7) can in the diffusion regime ($\mu_s{'} \gg \mu_a$) be approximated to

$$D \approx \left(3\mu_s{'}\right)^{-1}, \tag{9}$$

as discussed by Yamada et al.[27] The scattering coefficient μ_s and the anisotropy factor g do not appear separately in the diffusion equation. Different combinations of μ_s and g give the same solution as long as $\mu_s{'}$ is constant. This relationship is known as the similarity principle.[28] The two properties are therefore combined in $\mu_s{'}$,

which will be uniquely defined by the diffusion equation. The diffusion equation can be solved analytically for an infinite homogeneous medium. For other geometries the solution has also to fulfil the boundary conditions. Such solutions can be found for special cases, such as homogeneous media in certain simple geometries (see Chapter 2.3). More complex geometries, such as media containing absorbing or scattering bodies, have to be solved numerically.

2.3 Time domain solutions

For a short light pulse from an isotropic source, the transport through a turbid medium will cause a temporal broadening (Fig. 1). By measuring this broadening, it is possible to extract information about the tissue optical properties. Alternative measurement techniques to obtain these properties include frequency domain and spatially resolved steady-state measurements. Below, the mathematical tools to derive the optical properties from these types of measurements will be described.
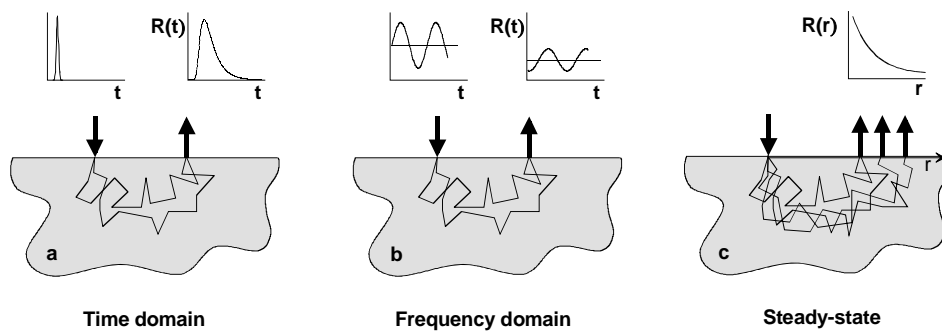

Fig. 1 Optical reflectance measurements of three types. (a) time domain, Chapter 2.3. (b) frequency domain, Chapter 2.4. (c) steady-state (spatially resolved) measurements, Chapter 2.6.

If the source is described as a delta function in time and space, $S(\mathbf{r},t)=\delta(0,0)$, the solution to the diffusion equation (8) in an infinite medium is

$$\varphi(\mathbf{r},t) = c(4\pi Dct)^{-3/2} \exp\left(-\frac{\mathbf{r}^2}{4Dct} - \mu_a ct\right). \qquad (10)$$

This Green's function can be used to determine the fluence rate in other simple geometries such as semi-infinite medium and homogeneous slab. If the light source is a collimated beam incident on the tissue surface, which is the case for most practical applications, we cannot assume an isotropic source on the surface. Patterson *et*

al.[29] have proposed that the source term in this case can be described as an isotropic source at a depth equal to the mean free path of isotropic scattering,

$$z_0 = \left(\mu_s{'}\right)^{-1} \tag{11}$$

Assuming that all incident photons are initially scattered at this depth will not yield any significant inaccuracies in fluence rates far from the source. We also have to specify an appropriate boundary condition for the interface between the tissue and air. The boundary condition should be that there is no photon flux from the surrounding air back into the tissue. It has been shown that setting the fluence rate to zero at an extrapolated boundary outside the real boundary is a convenient way of approximately fulfilling the boundary condition for an air–tissue interface.[1,24,30,31] This boundary is located a distance z_b above the surface, where z_b depends on the tissue diffusion coefficient D and the Fresnel reflection at the surface.[30] For an air–tissue interface, z_b is approximately $2z_0$.[1] However, the solution to the diffusion equation far from the source is insensitive to the exact location of the extrapolated boundary.[29] Hence, assuming a zero fluence rate on the actual surface (z_b=0) is a good approximation for such a situation. The boundary condition can be satisfied by adding a negative image source outside the tissue at a distance $2z_b+z_0$ above the surface (Fig. 2).
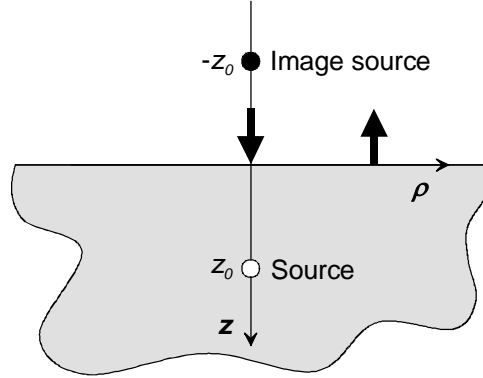

Fig. 2 Simplified boundary condition for a semi-infinite geometry. Isotropic point source z_0 into the medium an a negative image source at z_0 above the actual surface (z_b is here assumed to be zero).

The reflectance, $R(\rho,t)$ at an air–tissue boundary can be derived as[29]

$$R(\rho,t) = (4\pi Dc)^{-3/2} z_0 t^{-5/2} \exp(-\mu_a ct) \exp\left(-\frac{\rho^2 + z_0^2}{4Dct}\right),$$

(12)

where ρ is the source-detector distance. In a clinical situation, it is often interesting to measure the transmittance through a slab of tissue by placing the source on one side, e.g., of a compressed breast, and measuring the light transmitted on the other side. In this case, the boundary condition at the two tissue surfaces could be met by adding an infinite number of dipole sources mirrored in the two tissue boundaries. Retaining four dipoles will give the transmittance[29]

$$T(\rho,d,t) = (4\pi Dc)^{-3/2} t^{-5/2} \exp(-\mu_a ct) \exp\left(-\frac{\rho^2}{4Dct}\right)$$

$$\times \left\{ (d - z_0)\exp\left[-\frac{(d-z_0)^2}{4Dct}\right] - (d+z_0)\exp\left[-\frac{(d+z_0)^2}{4Dct}\right] \right.$$

$$\left. + (3d - z_0)\exp\left[-\frac{(3d-z_0)^2}{4Dct}\right] - (3d+z_0)\exp\left[-\frac{(3d+z_0)^2}{4Dct}\right] \right\},$$

(13)

where d is the thickness of the slab. Fitting the analytical solution of Equation (12) or (13) to a measured reflectance or transmittance curve will provide an estimate of the optical properties μ_a and μ_s'. This is often a quick and easy way to determine these properties *in vivo* on tissue or directly on a phantom in a laboratory environment (Papers I, II and III).

2.4   Frequency domain solutions

In the frequency domain, we instead consider a source which is intensity modulated with a sinusoidal signal at frequency f, angular frequency $\omega=2\pi f$. The detected light at a distance ρ away from the source will be both phase-shifted and amplitude demodulated with respect to the source. The phase shift ϕ and modulation M of the detected signal are related to the absorption and scattering characteristics of the tissue.

If the source varies in time as $S = S_{DC} + S_{AC}\exp(i\omega t)$, the fluence rate will have a DC and an AC component. In an infinite medium, the fluence rate can be expressed as[1]

$$\varphi(\mathbf{r},t) = A_{DC}\frac{\exp(-\mu_{eff}r)}{r} + A_{AC}\exp[i(\omega t - k_i r)]\left[\frac{\exp(-k_r r)}{r}\right]$$

(14)

where A_{DC} and A_{AC} are the DC and AC components of the source amplitude and μ_{eff} is the DC effective attenuation defined by

$$\mu_{\mathit{eff}} = \left(\frac{\mu_a}{D}\right)^{1/2} = \left(3\mu_a\left(\mu_a + \mu_s'\right)\right)^{1/2}. \qquad (15)$$

The complex wave number of the photon density wave launched by the source is $k = k_r + \mathrm{i}\cdot k_i$

$$k_r = \left(\frac{3}{2}\mu_a\mu_s{}'\right)^{1/2}\left\{\left[1+\left(\frac{\omega}{c\mu_a}\right)^2\right]^{1/2}+1\right\}^{1/2} \qquad (16)$$

$$k_i = \left(\frac{3}{2}\mu_a\mu_s{}'\right)^{1/2}\left\{\left[1+\left(\frac{\omega}{c\mu_a}\right)^2\right]^{1/2}-1\right\}^{1/2}. \qquad (17)$$

The real part of the wave number, k_r, governs the AC attenuation, while k_i is the phase lag per unit length. For the semi-infinite case, the modulation and phase shift have been derived, after applying an appropriate boundary condition, by Haskell *et al.* as[1]

$$M = \left(REAL^2 + IMAG^2\right)^{1/2}\left[\frac{\exp\left(-\mu_{\mathit{eff}}r_0\right)}{r_0} - \frac{\exp\left(-\mu_{\mathit{eff}}r_{0b}\right)}{r_{0b}}\right]^{-1} \qquad (18)$$

$$\phi = k_i r_0 - \arctan\left(IMAG / REAL\right) \qquad (19)$$

$$IMAG = \sin\left[k_i\left(r_{0b}-r_0\right)\right]\frac{\exp\left(-k_r r_{0b}\right)}{r_{0b}} \qquad (20)$$

$$REAL = \frac{\exp\left(-k_r r_0\right)}{r_0} - \cos\left[k_i\left(r_{0b}-r_0\right)\right]\frac{\exp\left(-k_r r_{0b}\right)}{r_{0b}} \qquad (21)$$

$$r_0 = \left(z_0^2 + \rho^2\right)^{1/2} \qquad (22)$$

$$r_{0b} = \left[\left(2z_b + z_0 \right)^2 + \rho^2 \right]^{1/2} \qquad (23)$$

$$z_b = \frac{2\left(1 + R_{\mathit{eff}}\right)}{3\mu_s{}'\left(1 - R_{\mathit{eff}}\right)} \qquad (24)$$

where r_0 and r_{0b} are the distances from the detector to the positive and negative image source centred around an extrapolated boundary. R_{eff} is the effective reflection coefficient for the boundary.[1] These equations have been used to evaluate the recorded data in Papers IV and V, dealing with frequency-resolved measurements at multiple frequencies.

2.5 Photon density waves

The similarities between the time and frequency domain methods to derive the optical properties is very relevant in this work (Paper II) dealing with photon density waves. Theoretically, there is a perfect correspondence between the time and frequency domains, and transitions from one domain to the other can be obtained through the Fourier transform.

When performing experiments in the time domain, an ultra short laser pulse is sent into the tissue. The pulse detected at some distance from the detector will be temporally broadened due to multiple scattering in the tissue. In the frequency domain, the light source is sinusoidally intensity modulated at some chosen modulation frequency. The group of travelling photons can be described as a diffuse photon density wave (DPDW), i.e. a wave of travelling light energy density inside the tissue. Microscopically, the photons are scattered back and forth inside the tissue and coherence is quickly lost, but macroscopically the photon density wave is travelling spherically out from the source, maintaining coherence many centimetres into the tissue. This wave will have a well-defined wavelength, amplitude and phase at all points. The detected signal will still be a sinusoidally varying light intensity at the initial modulation frequency, but the phase will be different and the amplitude lower. In the time domain, this would correspond to a delayed peak and reduced peak intensity, respectively. The amplitude and phase delay will be dependent on the optical properties of the tissue. It is important to keep apart the wave properties of the actual light and those of the photon density wave. The modulation frequency of the photon density wave is typically chosen to some hundreds of MHz, and its wavelength will in a typical tissue be in the order of a few centimetres.[32] The optical wave might have a wavelength somewhere in the optical window, for example at 800 nm, which corresponds to a frequency of $2.7 \cdot 10^{14}$ Hz. This wave is multiply scattered in the tissue, while the photon density wave is not. Thus, while travelling through the tissue, the photon density wave maintains coherence for a

reasonably long distance, in the order of a wavelength, and spatial information about the medium can be extracted.

2.6 Steady-state solutions

The optical properties of solid tissue can also be determined from steady-state diffuse reflectance measurements. The steady-state case of the diffusion equation (8) is given by

$$D\nabla^2\varphi(\mathbf{r}) - \mu_a\varphi(\mathbf{r}) = Q(\mathbf{r}), \tag{25}$$

where $Q(\mathbf{r})$ is a modified source term. The Green's function describing the fluence at a distance r from a point source at the origin in an infinite medium is

$$\phi(r) = \frac{1}{4\pi D}\frac{\exp(-\mu_{eff}r)}{r} \tag{26}$$

where μ_{eff} is the effective attenuation coefficient of the tissue defined by Equation (15). The reduced albedo, $a' = \mu_s'/(\mu_a + \mu_s')$ can be determined by measuring the total diffuse reflectance in steady-state, but the values of μ_a and μ_s' cannot be separated.[33] However, if the scattering coefficient is known or assumed to be constant, relative variations in μ_a with time or wavelength can be estimated. To determine absolute values of μ_a and μ_s', measurements of the local diffuse reflectance $R(\rho)$ at different distances ρ can be made (Fig. 1). In a semi-infinite medium, the local diffuse reflectance, being the flux out from the tissue surface, is given by Fick's law[30]

$$\begin{aligned}R(\rho) &= -D\nabla\varphi \\ &= \frac{1}{4\pi}\left[z_0\left(\mu_{eff} + \frac{1}{r_0}\right)\frac{\exp(-\mu_{eff}r_0)}{r_0^2} + (z_0 + 2z_b)\left(\mu_{eff} + \frac{1}{r_{0b}}\right)\frac{\exp(-\mu_{eff}r_{0b})}{r_{0b}^2}\right].\end{aligned}$$
$$\tag{27}$$

Here, an extrapolated boundary condition has been employed, and r_0 and r_{0b} are the distances from the detector to the positive and negative image source, given by Equations (22) and (23). For small distances from the incident beam, ρ on the order of a few transport mean-free path lengths, the magnitude of the diffuse reflectance is determined primarily by the transport scattering coefficient, μ_s'. This can be seen in Equation (27) as $\mu_{eff} \ll 1/r_0$ (and $1/r_{0b}$), and by recalling that $z_0 = (\mu_s')^{-1}$. The interpretation of this can be that the absorption will not influence this light to a great extent, due to the short optical path lengths involved. For large distances ($\rho \gg \mu_{tr}$), the radial local diffuse reflectance curve, Equation (28), is primarily determined by μ_{eff}, which is a function of both μ_a and μ_s'. The scattering and absorption

can be determined by combining the measured μ_{eff} , with the reduced albedo a' from a total diffuse reflectance measurement. Alternatively, the shape of the local reflectance curve in Equation (28) can be used, either by fitting the solution to a reflectance curve or by comparison to a data set of known reflectance curves. This data set can consist of either experimental or Monte-Carlo simulated reflectance curves.[34]

2.7 Absorption

The probability of light absorption by tissue molecules is described by the absorption coefficient μ_a [m-1]. As mentioned earlier, the absorption of light in tissue is strongly wavelength dependent, since different absorbing molecules, called chromophores, absorb in different wavelength regions. The absorbed energy is most often converted to heat, but can also be re-emitted as fluorescence or be used for a photochemical reaction. The wavelength dependence of the absorption coefficient for typical breast tissue is illustrated in Fig. 3. The spectrum in the figure was calculated by adding the absorption spectra of the contributing chromophores at realistic concentrations. The curve shape of absorption spectra measured *in vivo* on female breast tissue (Paper I) correspond well to in this figure.
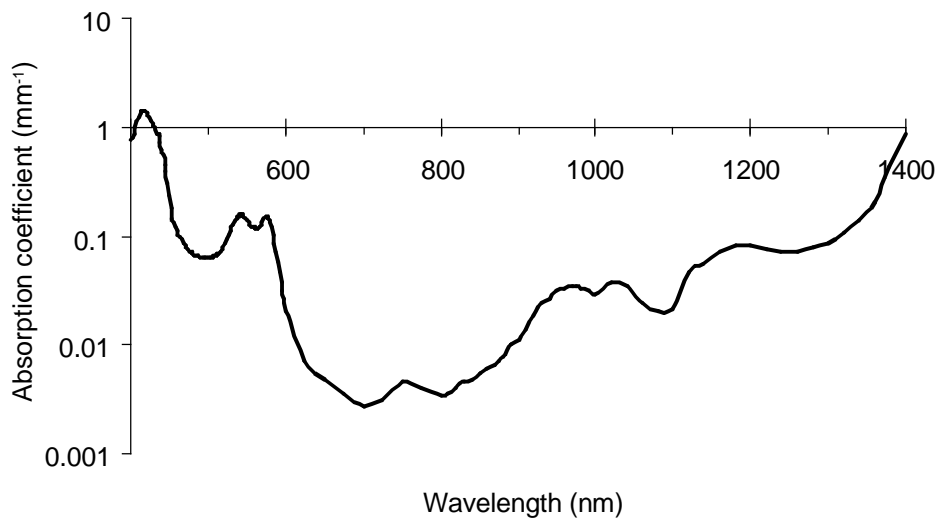

Fig. 3 Absorption spectrum of typical breast tissue as calculated using the absorption spectra of the contributing chromophores. In this case, oxy-and deoxy-haemoglobin concentrations of 20 μM and 10 μM, respectively, a fat concentration of 30 % and a water concentration of 70 % have been assumed.

Between approximately 600 nm and 1300 nm, the absorption is relatively low. At shorter wavelengths, haemoglobin absorption is large, and at higher wavelengths the strong water absorption drastically reduces light penetration. Light in this wavelength region, often referred to as the tissue optical (or therapeutic) window, is used for many diagnostic and therapeutic purposes, offering a possibility to reach targets deep into the tissue.[35] The most important absorbers in the visible and near-infrared wavelength region will be discussed in the following subchapters.

2.7.1 Water

Water is present in most soft tissues, in varying abundances. In skeletal muscle, for example, the water concentration is on an average 75 %, and in adipose (fatty) tissue it is approximately 20 %.[36] Water has a high absorption in the ultraviolet (UV) region up to about 200 nm wavelength. Further up in the UV, the absorption is low. At visible wavelengths up to approximately 600 nm, the absorption coefficient is even lower, less than 0.0001 mm^{-1}. Above that, it starts rising, with absorption peaks at approximately 975 nm, 1200 nm, 1440 nm and several more peaks further out in the infrared (IR). [37] Above approximately 950 nm, water dominates the absorption spectrum of most soft tissues.
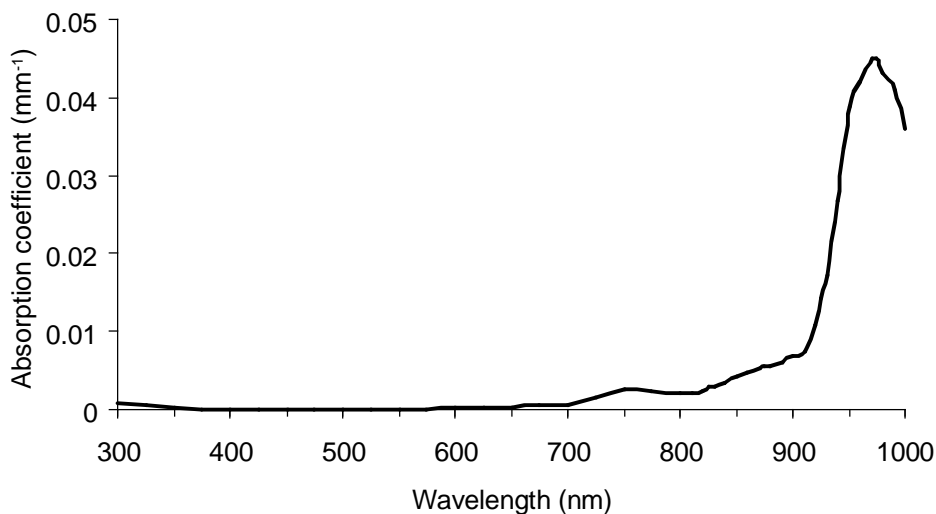

Fig. 4 Absorption spectrum of pure water.[37,38]

2.7.2 Haemoglobin

Haemoglobin, which is the iron-containing pigment serving as the oxygen-carrier in the red blood cells, has a very high absorption in the visible wavelength region.

The binding of oxygen to the haemoglobin molecule markedly changes its three-dimensional structure and this, in turn, affects the light absorption. Haemoglobin is the strongest absorber in human tissue. However, the concentrations in soft tissues is usually only in the order of a few percent of volume. The absorption of the oxygenated (HbO_2) and deoxygenated (Hb) forms have different spectral features (Fig. 5). Oxy-haemoglobin has its highest peak at approximately 414 nm, and two lower peaks at 542 and 577 nm. The absorption peak of deoxy-haemoglobin is shifted towards a longer wavelength, 433 nm, and a single peak at 556 nm replaces the double peaks in the green wavelength region of the oxy-haemoglobin spectrum. Deoxy-haemoglobin also has a small absorption peak at 760 nm not found in oxy-haemoglobin. These differences in spectral features between oxy- and deoxy-haemoglobin can be used to measure changes in haemoglobin saturation, as is now routinely done in clinical practise by pulse-oximetry.[39-41] It is worth noting that at some wavelengths, the absorption of oxy- and deoxy-haemoglobin are equally strong. These so called isobestic points are at approximately 390, 422, 452, 500, 530, 545, 570, 584, and 797 nm, and they can serve as reference points in tissue oxygenation measurements.

Myoglobin is a haemoglobin-like pigment, which serves as an oxygen carrier in muscle tissue. Deoxygenated myoglobin has an absorption spectrum that is virtually indistinguishable from deoxygenated haemoglobin. Oxygenated myoglobin is very similar to oxygenated haemoglobin in the near-infrared, but differs strongly in the wavelength region between 500 and 650 nm, where it lacks the two absorption peaks of oxy-haemoglobin.[42]
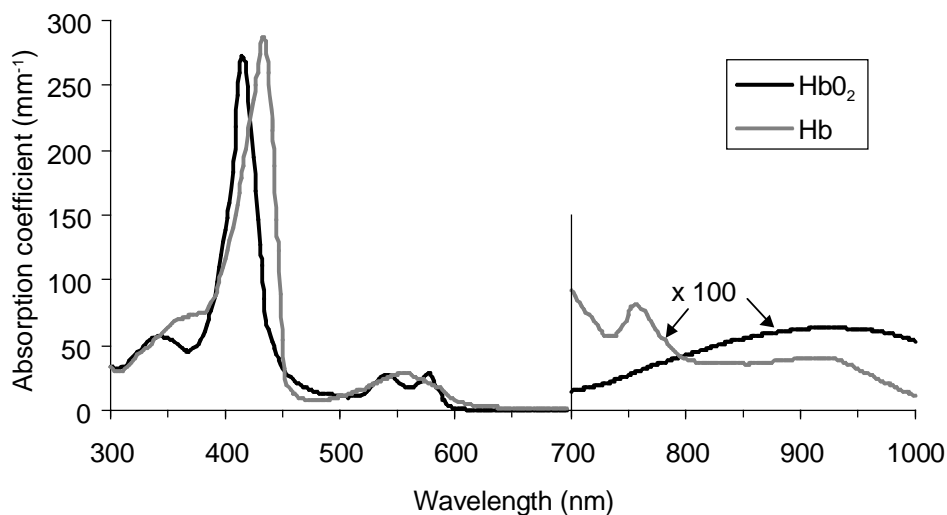

Fig. 5 Absorption spectra of oxy- and deoxy-haemoglobin, both at a concentration of 150g/liter of blood.[38]

2.7.3 Lipids

Lipids have a low absorption in the visible wavelength region, but in the NIR region it cannot be neglected in all tissues. The percentage body adipose tissue averages to approximately 18 % and 29 % in the normal male and female, respectively.[43] Female breast tissue, considered in Papers I, V and VI, consists to a large extent of adipose tissue. The amount of adipose tissue in breast varies considerably between individuals, depending on age, hormonal status and general build of the woman. Adipose tissue consists to about 70 % of lipids, stored as fat droplets that occupy most of the volume of the large adipose cells. The absorption spectrum of fat as measured with a spectrophotometer can be seen in Fig. 6. It has a high peak at approximately 930 nm and a lower at 760 nm, where also deoxyhaemoglobin absorbs, as mentioned above. The fat contents of breast tissue can be estimated by taking advantage of the high absorption of fat above 900 nm, as described in Paper IV. White adipose tissue, which is the most abundant type of adipose tissue in the body, varies in colour from white to yellow. This depends in part on carotenoids, which accumulate in the lipid droplets of the adipose cells. The shape of the absorption spectrum of β-carotene is also shown in Fig. 6. β-carotene has a high absorption around 450 nm, but the absorption drops off at about 500 nm and stays low and almost constant between 600 and 1000 nm.
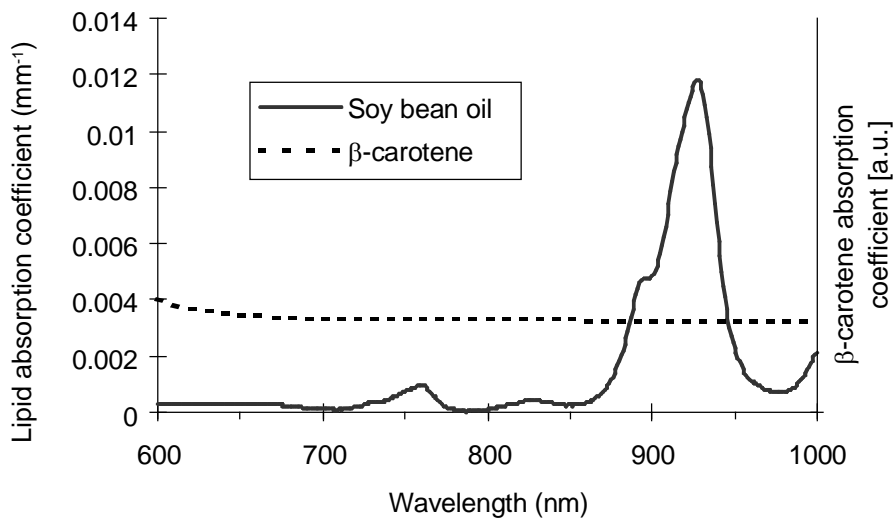

Fig. 6 Absorption spectra of soy bean oil and β-carotene, as measured with a spectrophotometer. The β-carotene spectrum shown is not to scale. From Paper IV.

2.7.4   Melanin

Melanin is a dark pigment which accounts for most of the light absorption in (and thus gives the colour to) hair, skin, and the iris in the eye. Two groups of melanin exist, eumelanin, which is a black-to-dark-brown pigment, and pheomelanin, which is a yellow-to-reddish-brown pigment found in red hair. Melanin is synthesized in the melanosome, an organelle of roughly 1 µm diameter. Melanosomes may contain a variable amount of melanin, and variation in absorption values of melanin can be tenfold. The spectrum shows no sharp features, and the attenuation decreases exponentially with the wavelength. This attenuation spectrum may be due to a combination of Rayleigh scattering and absorption. The measurement of light extinction in melanin is difficult, since it is insoluble and one cannot extract it from the skin without changing its properties. However, an approximate attenuation spectrum of melanosomes in skin can be seen in Fig. 7.[44]
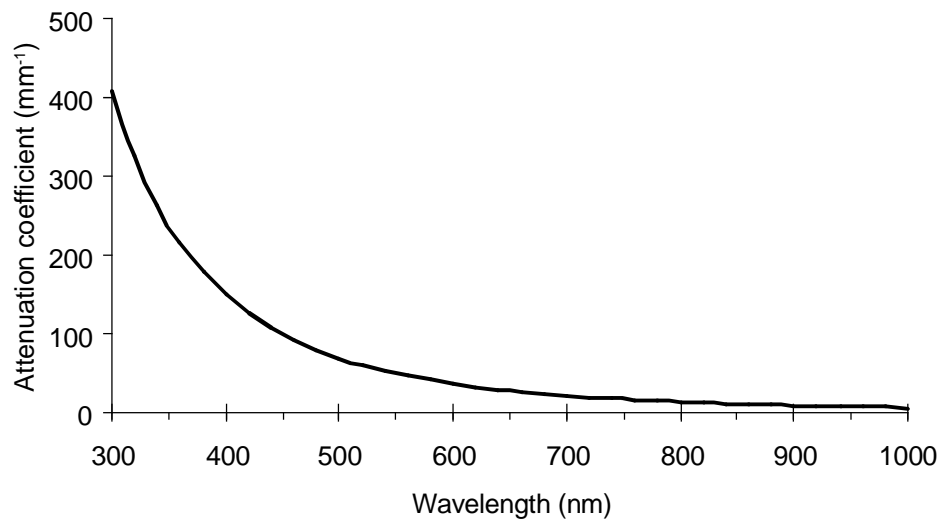

Fig. 7 Attenuation spectrum of melanosome in skin. After Jacques et al.[44]

2.7.5   Other chromophores

At wavelengths in the ultraviolet and blue region, proteins and amino acids absorb strongly.[35] Some also exhibit fluorescence. Collagen, for example, which is a family of fibrous proteins abundant in most organs, absorbs light in the ultraviolet and fluoresces in the blue. Other chomophores may also absorb light, but they contribute only very little to the total light absorption of tissue, due to low abundance or absorption cross section.

2.8 Scattering

The wavelength dependence of the scattering properties of tissue is not as strong as for the absorption. The scattering coefficient μ_s [m^{-1}], which is the probability of scattering per unit length, decreases with light wavelength, and the spectrum has no sharp features as can be seen in Fig. 8. In soft tissue μ_s is typically in the order of 10 mm^{-1}, so that the scattering mean free path is in the order of 0.1 mm. As mentioned above, tissue scattering is not isotropic, but strongly forwardly directed, and typical values of the anisotropy factor g measured *in vitro* in mammalian tissues are in the range 0.7–0.95.[45] A typical value of g in the wavelength region of the optical window is 0.9. Hence, the reduced scattering coefficient, μ_s' is usually in the order of 1 mm^{-1}.
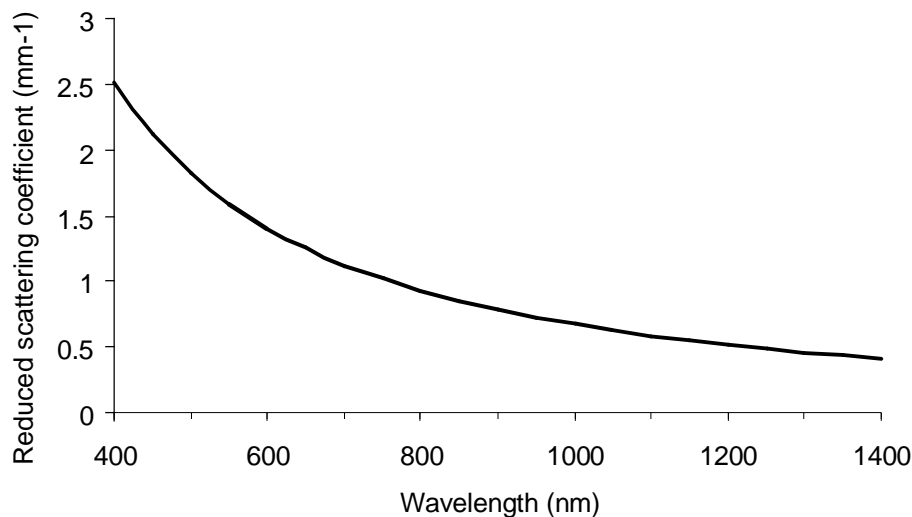

Fig. 8 Reduced scattering coefficient of typical tissue as calculated by linear extrapolation of an exponential fit to data from Paper IV.

2.8.1 Microscopic contributors to light scattering in tissue

Whereas absorption depends on biomolecules in the tissue, scattering is due to larger microscopic structures such as spatial variations in refractive index. The macroscopic average refractive index of most tissues lies in the 1.38-1.41 range at 633 nm wavelength, with an approximate decrease of 1 % per 100 nm in the visible region.[46,47] Adipose tissue is an exception, having a refractive index of approximately 1.46. However, looking at the tissue on a microscopic level, the refractive index varies spatially, with lower refractive index in the cytosol, which mainly is an aqueous solution of salts and proteins, n=1.38, and higher in the membrane struc-

tures, n=1.48, which consist of phospholipid bilayers.[48] Possible scattering centres in tissue are the cell nucleus, the mitochondria, the cell membrane or other cell organelles such as lysosomes or Golgi apparatus. It has been shown that the majority of the scattering is due to structures within the cell rather than the cell membrane.[49] The size of the scattering centres can be estimated by comparison with Mie scattering theory,[50-52] or by examining the spatial variations in refractive index by phase microscopy.[48] The cell membrane has been found to be responsible for the scattering at small angles, the nucleus is responsible for scattering at slightly larger angles, while more isotropic scattering is due to smaller organelles within the cell, such as mitochondria.[51] Hepatocytes in liver tissue have a very high mitochondrial content, and a correlation between reduced scattering coefficient and mitochondrial content has been found.[49] The large scattering contribution from the mitochondria in liver tissue has been confirmed by comparing Mie theory to integrating sphere measurements.[52] Fibrous structures such as collagen and elastin also influence the scattering,[53] as well as lipid droplets.[49,54] The scattering properties of fat have been shown in Paper IV to be highly dependent on tissue temperature, and the reduced scattering coefficients obtained *in vitro* will most probably not agree with values measured *in vivo*.

Chapter 3
Optical diagnostics using
photon density waves

For the planning of both diagnostic and therapeutic laser methods, it is important to know the optical properties of the tissue at the chosen wavelength. There are different methods available for determination of the scattering and absorption properties of a turbid medium, among them integrating sphere measurements for thin *in vitro* samples,[55] spatially resolved measurements,[34] and time- or frequency-resolved transmittance or reflectance measurements.[29,56] As seen in the previous chapter, it is impossible to extract the μ_s and g factors independently if the light has been diffusely scattered before detection. In practice, only integrating sphere measurements can determine both μ_a, μ_s and g, but not always with high accuracy. Integrating sphere measurements require thin samples, and can thus usually only be performed *in vitro*. The other methods mentioned measure diffuse light, and thus yield μ_a and μ_s' only, but can be performed both *in vitro* and *in vivo* and on thick samples. Studying the propagation of photons in tissue can yield information about optical properties and, indirectly, sense the presence and possibly the type of tumours or detect haemorrhage.[57] The main applications are today envisioned to be detection of breast tumours, certain brain injuries, and measurements of tissue physiology such as blood volume and haemoglobin oxygenation. The projects presented in this thesis have aimed at breast measurements. Imaging techniques are best suited for breast tumour detection, while spectroscopy using one source and one detector might be sufficient for measurements of tissue physiology. This chapter outlines the medical background and describes some techniques for *in vivo* breast measurements, in particular those used in Papers I-V. The time-correlated single photon counting technique used in Papers II and III is not discussed in the manuscripts, and is therefore described in more detail here.

3.1   Medical background

Breast cancer is the most common cancer among women, accounting for more than 25 % of all female cancers. It is estimated that 10 % of all women will develop a breast cancer at some time during their lives.[58] Today, there is a need for improved detection of breast tumours. Early diagnosis of breast cancer increases the chances of successful treatment.[59]

The parenchyma, or functional part, of a breast consists of lobules, where milk is secreted during lactation, and a branching duct system leading from the lobules radially in to the nipple. The lobules and the ducts are supported by fibrous tissue, and all this is distributed within the adipose tissue of the breast (Fig. 9). The amount of breast adipose tissue varies greatly between individuals and in one individual depending on age, hormonal status, etc (Paper V).[60] However, the difference between the right and left breast in the same woman seems to be smaller (Paper I). In a clinical situation, using the contralateral breast as a control could therefore be a good approach. Younger women have more fibrous breasts whereas elder women usually have predominantly fatty breasts. Tumours in fibrous breasts are usually more difficult to find by x-ray mammography than tumours in fatty breasts. One niche of optical tomography could therefore be the examination of young women. Women who are sensitive to x-rays or who are genetically predisposed for breast cancer could be examined more often with a harmless optical technique.[61] Optical diagnostics of breast tissue is based on variations in the diffusely reflected or transmitted light, possibly due to differing optical properties of the tumour itself but more probably to the host response to the cancer.[60] An *in vitro* study shows that the differences in optical properties between normal and different types of diseased tissue are not significant.[6] However, since these measurements were performed *in vitro*, absorption is underestimated. The study showed significant differences in optical properties between healthy and diseased tissue in the same patient. Again, this indicates that a baseline for each individual could be established by measurements on the healthy breast. Invasive ductal carcinoma is the most common form of breast cancer.[59] Carcinomas are often surrounded by inflammatory cells and new blood vessels, which form a network around the tumour periphery. In addition, the cancer cells are usually surrounded and supported by dense fibrous tissue, which is rich in collagen, water and haemoglobin but with almost no fat. These host responses are believed to be the most probable source of contrast for optical techniques.[60] It has been shown that the contrast can be improved by using indocyanine green (ICG) as a contrast agent.[41] It can be given intravenously and shows a preferential uptake due to the vasculogenesis of tumours. It has an absorption maximum in the near-infrared at 805 nm, and emits fluorescence at approximately 835 nm.
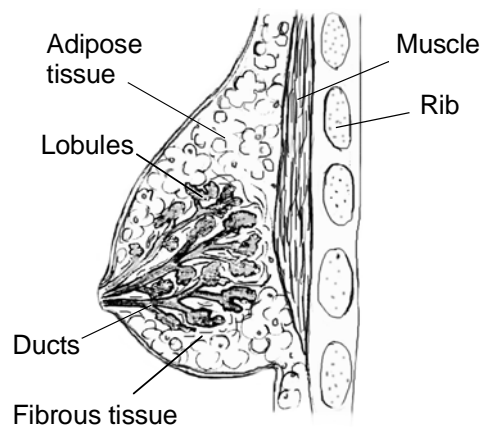
Fig. 9 Anatomy of the female breast. Glandular tissue (lobules and ducts supported by fibrous tissue) is embedded in adipose tissue.

Since the variability in normal breast tissue optical properties is so large, it is important to understand these variations before attempting to detect tumours. The breast measurements presented in this thesis are almost exclusively on healthy tissue.

When performing pre-clinical studies of optical diagnostic methods, it is often practical to work with a tissue phantom instead of real tissue. White Delrin plastic has a high scattering, approximately 2.3 mm^{-1} at 670 nm, and a low absorption, 0.002 mm^{-1} at the same wavelength.[62] It is durable and easy to handle. The disadvantages are that the optical properties are fix and that it can be difficult to insert tumour phantoms. Another common tissue phantom is Intralipid, which is a white fat emulsion, normally used as an intravenously administered nutrient. It can be diluted to the required scattering properties and ink can be added for absorption.[63,64] Tumour phantoms can easily be immersed, and agar powder can be added to make the Intralipid phantom more solid.[65] Clear resins with absorbing dyes and scattering silica or quartz spheres have also shown to be reproducible and optically accurate.[66,67] Other substances, for example milk and polystyrene microspheres, can also be used as optical tissue phantoms.

3.2   Determination of optical properties by time-resolved measurements

Diffusion theory in the time domain has been described in Chapter 2.3. After pulsed irradiation, the time of photon escape from the tissue is related to photon path. By observing the time distribution of detected photons, inhomogeneities bur-

ied in the tissue can be detected. In most realistic tissue geometries, there is no ballistic, or nonscattered, component. In a transmission geometry, the first arriving photons can be considered as quasi-ballistic, i.e. less scattered than the later ones. A sharper image of objects hidden inside the tissue can be accomplished by looking at the quasi-ballistic photons only, so called time-gated viewing.[57,68,69] It has been shown that time-gated viewing is more sensitive to changes in scattering than to absorption properties.[70] In the time dispersion curve, an increased scattering will mainly affect the time to maximal signal, t_{max}, while an increased absorption will give a steeper exponential slope at longer times. In a reflectance geometry, the first arriving photons have not penetrated as deeply into the tissue as the later ones. Photons going deeper into the tissue arrive later, and different depths can be probed using time-gated detection.

The time-correlated single photon counting technique, used in Papers II and III, is based on a short-pulsed high repetition-rate laser light source and a photon-counting detector setup.[69,71] Fig. 10 shows the time-correlated single photon counting system used in Papers II and III. The light source is an Ar-ion laser pumped mode locked Ti:Sapphire laser (Coherent Mira 900) operating at 790 nm with approximately 100 fs long pulses. Optical fibres are used for delivering light, both from the source to the sample and back to the detector. The light pulse is sent into the medium, and the time delay between the first detected transmitted photon and a reference pulse is measured and converted by a time-to-amplitude converter (TAC) to a voltage proportional to the time delay. In a multi-channel analyser, the count in the channel corresponding to this voltage (or time difference) is increased by one. The procedure is repeated, yielding statistics for the time delay of the emerging photons. The histogram obtained is equal to the time dispersion curve. The drawback of this technique is that it is relatively time consuming. As the detection is based on statistics, a sufficient number of photons has to be detected to give a reasonably noise-free curve. However, only a limited number of photons can be detected per second due to pile up. This can occur when the probability of detecting one photon per excitation pulse is close to 1, and thus, the probability of receiving two photons from the same excitation pulse at the detector is not negligible. In that case the electronics can handle only the first arriving photon and the second will not be registered. This will introduce an error in the photon statistics.

3.3   White light examination of tissue

Time-resolved measurements can be used to determine the absorption and reduced scattering coefficients in a wider wavelength range if a pulsed white light source is used (Paper I).[72] Ultra-short white light pulses were created by focusing pulses from a high-power laser into a cuvette of water. The nonlinear part of the refractive index of water caused a frequency shift in the light pulses. This shift is
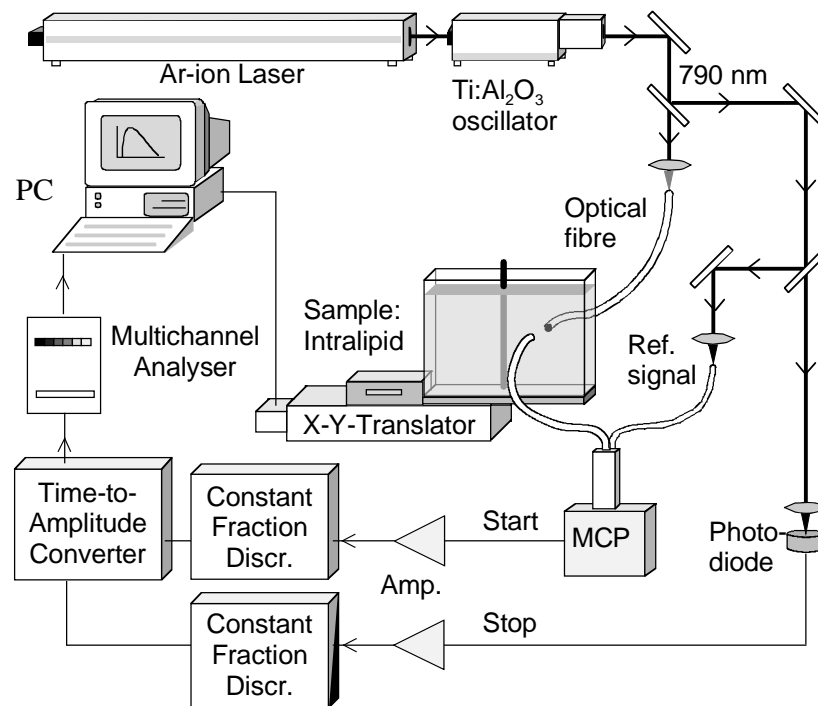
Fig. 10 Time-correlated single photon counting setup, used in Papers II and III.

proportional to the time derivative of the light intensity, and will thus vary during the pulse. White light, containing light in the entire visible and near-infrared wavelength region, was created.[73] This process is called self-phase modulation. The short pulses of white light were used to perform back-scattering measurements *in vivo* on the female breast (Paper I). A polychromator and a streak-camera were used for detection. This detection system yielded time dispersion curves in a broad wavelength region. By fitting solutions to the expression for the diffuse reflectance $R(\textbf{\textit{r}},t)$, given by the diffusion equation, to these curves as described in the previous chapter, the absorption and reduced scattering in the tissue can be determined for all wavelengths of interest from one single recording. In Paper I, white light measurements were performed *in vivo* on female breast tissue, to determine its optical properties in a wide spectral range. These recordings covered the wavelength region from approximately 670 to 830 nm.

3.4 Interfering photon density waves

Highly sensitive detection of small inhomogeneities in scattering media can be obtained by exploiting the destructive interference between two light sources (cancellation technique). This technique was suggested by Knüttel et al.[74,75] and has been explored further and used for imaging by Chance et al.[76,77] Images can be obtained by a phased array setup, where an array of sources of different relative phase is used. A similar technique is used for medical ultrasound, where the signal can be focussed in a particular spot by changing the relative phase of a large number of sources.

In the studies presented in Papers II and III the cancellation technique was used in a transmission geometry. The measurements were performed in the time domain, using a time-correlated single photon counting setup, as shown in Fig. 10, but the analysis was performed in the frequency domain, following Fourier transformation. The method is based on the principle of two intensity-modulated light sources placed on the surface of a homogeneous turbid medium, such as a perfectly homogeneous tissue. The detected signal in any point in the tissue will be the sum of the contributions from the two sources. Consider that these sources are modulated with the same intensity and at the same frequency, but at 180° phase difference. Assume now that there is a detector placed in a point equidistant from the two sources. At this position there will be destructive interference at the modulation frequency, and the amplitudes will add up to zero due to the 180° phase difference. The detector placed midway between the sources will thus be very sensitive to small asymmetries or changes in the optical properties of the medium. If the whole arrangement with sources and detector is scanned over a tissue slab, an object with optical properties different from those of the tissue, such as a tumour, will cause an amplitude minimum and an abrupt 180° phase shift as it passes the detector. The results from such a measurement can be seen in Fig. 11.

In Papers II and III, measurements of interfering photon density waves performed in the time domain are described. The Fourier transform links the two domains together, and an infinitely short light pulse can be transformed to a wave containing all frequencies. In addition, a time shift in the time domain corresponds to a phase shift in the frequency domain. If two light pulses, with a well-defined time shift corresponding to 180° at some chosen modulation frequency, are sent through the tissue, the resulting time dispersion curve can be Fourier transformed to yield the same result as if a frequency-resolved setup was used. However, the signal-to-noise ratio is worse, since only part of the available light is used for this modulation frequency.
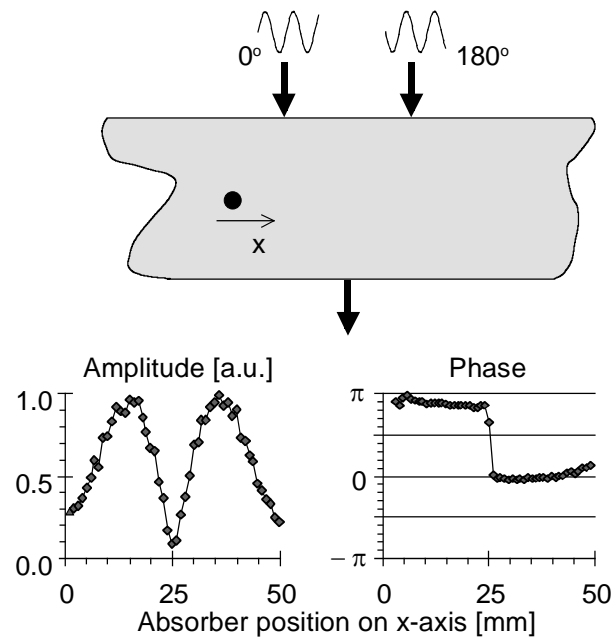
Fig. 11 Results from a scan across an Intralipid and ink sample ($\mu_a=$ 0.06 cm^{-1}, $\mu_s'=7$ cm^{-1}), containing a 4 mm cylinder of Intralipid, ink and agar. The sources are placed at x=10 mm and x=40 mm. The absorber has 4 times the absorption but the same scattering as the surrounding liquid. The frequency is 200 MHz. (From Paper II)

Moreover, as shown in Paper II, the measurements with the two pulses can be made separately. First a measurement is performed with the source fibre placed at a certain distance off the detector axis. Then the source fibre is moved to the position equidistant to the detector axis on the other side, and the measurement is repeated. The resulting time dispersion curves can be added together afterwards, and the time shift chosen arbitrarily. The fact that this is an additive effect opens the possibility to reverse the setup. This setup consists of one source and two detectors instead of two sources and one detector, see Fig. 12. The result will be the same irrespective of whether the light travels in one direction or the opposite. Two measurements are performed with the detector in the positions equidistant from but on opposite sides of the source axis. The two measured curves are added together, after achieving the desired phase shift between them by applying a time delay to one of them. All this is performed at computer analysis level. Hence from only two time-resolved measurements, the interference can be studied at any modulation frequency just by varying the time shift between the two pulses before adding them together.
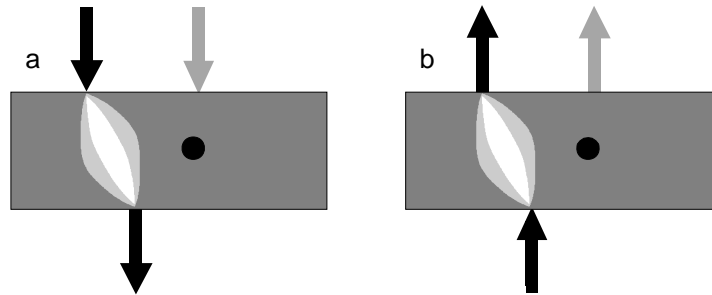
Fig. 12. (a) Normal and (b) reverse setup for interfering photon density wave experiments.

An arrangement with several detectors positioned in a two-dimensional pattern can also be used. By combining the detectors in different ways at the analysis phase, the plane of destructive interference can be constructed in different directions. Then an absorbing object hidden inside the sample can be more efficiently localized. A system developed by Chance *et al.* employs nine diode laser sources each at 750 nm and 830 nm wavelength and 4 detectors.[41] A 1 ml capsule of blood could be detected in a 12 cm thick breast model using 50 MHz phased array instrument. They claim that the system provides a high signal-to-noise ratio in a shorter time than required for normal frequency-resolved measurements.

3.5 Frequency domain photon migration

Fourier transforming a measured time dispersion curve will yield the response in terms of a phase delay and a demodulation of the signal for many frequency components (Papers II and III). In a frequency-resolved measurement, the measured phase shift and modulation, expressed by Equations (18) and (19) in Chapter 2, depend on the scattering and absorption as well as on the modulation frequency ω and the source-detector distance ρ. The phase shift increases and the modulation decreases with increasing μ_s', decreasing μ_a, increasing ω and increasing ρ. At higher modulation frequencies, the attenuation of the photon density wave is larger, and the probed volume is smaller.[78] If measurements are made in a reflectance geometry, the most probable photon path moves closer to the surface with increasing modulation frequency. This could be useful when measuring homogeneous media with a hidden absorber or layered media.[42,79] In the time-resolved case, this would correspond to an early time gate suppressing longer photon paths. It is in principle possible to determine the absorption and scattering coefficients by measuring the amplitude and phase at one modulation frequency only. Tromberg *et al.* have shown that by measuring at multiple frequencies, the influence of noise is reduced and the recovered coefficients are more reliable.[78] A portable frequency

domain photon migration (FDPM) system operating at modulation frequencies from 300 kHz to 1 GHz and at several light wavelengths were developed by Madsen *et al.*[80] This instrument was used in Papers IV and V for measurements of optical and physiological properties of female breast tissue. The broad bandwidth of this instrument allows μ_a and μ_s' in typical tissues to be quantified with a high accuracy.

Also images can be obtained using the frequency domain technique, either by scanning a source-detector setup in transmittance or reflectance geometry, or by using detector arrays.[81] Gratton *et al.* published the first frequency domain images of tissue, by scanning a source-detector arrangement in transmission geometry over a hand.[82] O'Leary *et al.* presented experimental frequency domain images of turbid media containing scattering and absorbing bodies, and showed by simulations that a higher modulation frequency will yield better image quality in a medium with low absorption, while in a higher absorption medium the image quality was independent of frequency.[77]

3.6 Measurement of physiological properties

The absorption of different tissue biomolecules has been discussed in Chapter 2.7. The spectral features of these molecules allow their quantification by spectrally resolved measurements. This has in particular been used to determine the haemoglobin oxygenation in tissues, usually employing one wavelength on each side of the isobestic point for haemoglobin at about 800 nm.[83-85] The data analysis has to account for the influence from scattering, giving different average path lengths *<L>* at different light wavelengths. Generally speaking, *<L>* increases with increased scattering and decreases with increased absorption. In the simplest case of haemoglobin absorption measurements, where $\mu_s'(\lambda_1) \approx \mu_s'(\lambda_2)$ and $\mu_s' \gg \mu_a$, it can be assumed that the path length is the same at the two wavelengths. The diffuse reflectance and transmittance depend on the path length as $R, T \sim \exp(-\mu_a <L>)$. The relative absorption is then given by[86]

$$\frac{\mu_a(\lambda_1)}{\mu_a(\lambda_2)} = \frac{\ln R(\lambda_2)}{\ln R(\lambda_1)}. \tag{28}$$

If the chromophores contributing to the absorption at a certain wavelength are known, the total absorption coefficient is

$$\mu_a(\lambda) = \sum_{chrom} \varepsilon_{chrom}(\lambda) C_{chrom}, \tag{29}$$

where $\varepsilon_{chrom}(\lambda)$ is the extinction coefficient of a chromophore at a certain wavelength, usually given in $cm^2 mol^{-1}$, and C_{chrom} is the concentration of the chromo-

phore in the tissue. If blood is the dominant absorber at the two wavelengths measured, the oxygenation $Y=C(HbO_2)/(C(Hb)+C(HbO_2))$ can be determined from Equations (29) and (30). The assumption that the scattering is wavelength-independent and constant among patients is traditionally used for example in pulse oximetry. In many cases, however, these assumptions do not hold and will yield inaccuracies in the estimated oxygenation. Measurements separating μ_s' from μ_a then have to be performed. This can be made in the time or frequency domain. It can also be done in steady-state, separating the scattering and absorption by spatially resolved measurements as described in Chapter 2.6. In the time domain, the optical properties can be obtained by fitting solutions to the diffusion equation to experimental time dispersion curves, as mentioned previously, or by looking at the terminal slope of $\ln R(\rho,t)$, since

$$\lim_{t \to \infty} \frac{\partial}{\partial t} \ln R(\rho,t) = -\mu_a c, \tag{30}$$

where c is the speed of light in the medium. In the frequency domain case, the phase shift is proportional to the path length, provided that the modulation frequency is low, $\omega \ll \mu_a c$. At higher frequencies, the phase shift does not describe the true path length, and the relationships become more complex. The measurement signal-to-noise ratio is also worse at higher frequencies, due to higher attenuation.

By making absolute measurements of μ_a at many wavelengths, Equation (29) can be used to determine the concentrations of tissue chromophores. Oxy- and de-oxy haemoglobin and water concentrations have been determined in normal and malignant tissues *in vivo* using multi-frequency measurements at four light wavelengths (Paper V).[87,88] This method has been developed further to enable the determination of lipid content in breast tissue (Paper IV). The absorption and reduced scattering coefficients were determined by nonlinear fits to the diffusion equation solution. The chromophore concentrations were then obtained from the least squares solution to the matrix form of Equation (29)

$$C = \left(\boldsymbol{\varepsilon}^T \boldsymbol{\varepsilon} \right)^{-1} \boldsymbol{\varepsilon}^T \boldsymbol{\mu}_a, \tag{31}$$

where C is a vector containing the chromophore concentrations, $\boldsymbol{\varepsilon}$ is a matrix containing the extinction coefficients of all chromophores at all wavelengths used, and $\boldsymbol{\mu}_a$ is a vector with the absorption coefficients measured at different wavelengths. In order to separate the contributions from different chromophores to the absorption, the light wavelengths have to be chosen properly. Fig. 13 shows the absorption spectra of oxy- and deoxy-haemoglobin, lipid and water, which are the main absorbers in breast tissue in the NIR wavelength range.
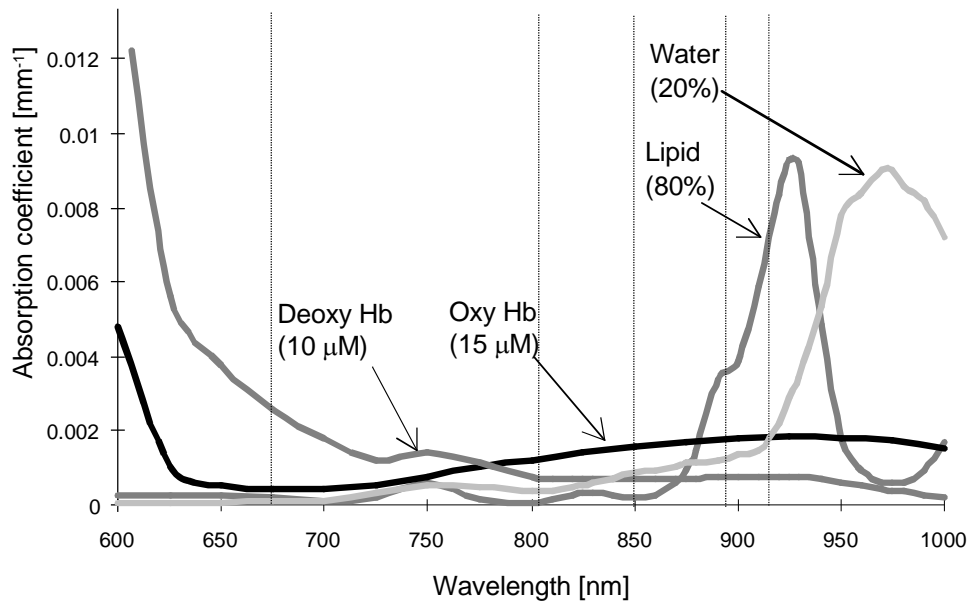
Fig. 13 Absorption spectra for breast tissue chromophores in the red and near-infrared wavelength region. Wavelengths measured by FDPM indicated. From Paper IV.

The wavelengths employed for the breast measurements by FDPM in Paper IV are indicated in the figure. The isobestic point for haemoglobin is close to 803 nm, and this wavelength together with 674 nm and 849 nm will determine the oxy- and deoxy-haemoglobin concentrations, and hence the blood volume and haemoglobin saturation. At 894 and 915 nm, water and fat are the main absorbers. However, the extinction coefficients at 894 nm have a strong correlation to those at 915 nm, and do not yield much additional information. Hence, 849 nm and 915 nm were used for separation of fat and water in Paper IV. An additional wavelength above 950 nm would probably improve the performance, but such a laser diode was not available during this particular study.

Measurements of chromophore concentrations in breast tissue have also been performed in the time domain by Cubeddu *et al.*[89] and in steady-state by Quaresima *et al.*[90]

Chapter 4
Fluorescence diagnostics of tumours

Laser-induced fluorescence (LIF) diagnostics is a spectroscopic method, which can provide information on the biochemistry and indirectly on the pathology of the tissue. The main advantages with LIF are that the measurements are safe and non-invasive and can be performed in real-time during a clinical examination. Research concerning the possibility of using LIF for diagnostics of different types of biological tissue has been studied extensively for many years.[23,91,92] The excitation light used for fluorescence measurements is usually in the near-UV or blue wavelength region, where penetration in tissue is short. Hence, fluorescence measurements are used for superficial lesions, as compared to the methods described in the previous chapter where light in the optical window was used for measurements of deeper lying lesions.

Papers VI to X concern *in vivo* fluorescence measurements from tissue. This chapter aims at describing the physical and medical background to tissue fluorescence. Specifically, applications to the colon and larynx will be discussed, since these organs are studied in Papers VI to IX. Fluorescent tumour marking substances will be discussed, as well as some aspects of fluorescence imaging (Paper X).

4.1   Medical background and motivation

The conventional methods for morphological characterization of lesions are mainly based on histopathology. Small pieces of tissue, or in some cases whole lesions, are excised and analysed by microscopy after thorough preparation. Histopathology is fairly reliable; studies have shown more than 90% agreement between pathologists classifying colorectal samples.[93,94] The main disadvantages are the risk of sampling errors, and the cost and time required for histopathological diagnosis. The results are usually not available until up to several days after the examination. In some cases, e.g. on the vocal folds, each biopsy will also prolong the healing time of the tissue. In further other applications, e.g. on heart tissue, biopsy sampling might be risky. Various alternative or complementary techniques, capable of providing diag-

nostic information in real-time during examination, are therefore under development and evaluation. Ultrasonic and optical techniques are such examples. Optical techniques have a unique potential in that they do not only rely on tissue morphology but also on physiology. If fluorescence could be used as a complementary method to yield cheap information noninvasively in real-time during the examination, it could therefore be of great interest in many clinical specialties. It could be used as a complement to ordinary biopsies, and to help the physician to find the most relevant sites for biopsy sampling. This would hopefully reduce the sampling error and help avoid unnecessary biopsies.

Laser-induced fluorescence of tissue is sometimes referred to as *optical biopsy*. This term is somewhat contradictory, since the word biopsy indicates that a tissue sample has to be removed, while fluorescence in itself is noninvasive and the objective is to obtain *in vivo* diagnostics.

When comparing results from different studies, it is important to consider if the measurements were performed *in vivo* or *in vitro*. The trauma when a tissue sample is removed will cause an immediate increase in haemoglobin absorption. At later times after resection, a decrease in NADH fluorescence significantly changes the spectral shape.[94] There are also other issues to consider when classifying different fluorescence methodologies. Fluorescence measurements can either be performed by point measurements or in an imaging geometry. In addition, LIF can either utilize the differences in autofluorescence, i.e. the natural fluorescence from the tissue itself, between normal and diseased tissue, or the fluorescence from a tumour marker, a substance that to a certain degree is accumulated selectively in premalignant and malignant tissue and that has a strong and characteristic fluorescence emission. These topics will be discussed later in this chapter.

4.1.1   Colon

The colon, or large intestine, is about 1.2 metres long and lies like an arch inside the abdomen from the ileum, or small intestine, to the rectum. Its primary function is the absorption of water and electrolytes and the storage of undigested material. The colon is lined with a columnar epithelium, which is a single layer of tall cells that are separated from the underlying connective tissue, called *lamina propria*, by a thin basement membrane (Fig. 14).

Colorectal carcinoma is the second most frequent malignancy in the United States.[58] Some other common pathologies in the colon are inflammatory bowel diseases, e.g. ulcerative colitis and Crohn disease, and neoplastic polyps. It is often difficult to establish a precise diagnosis without a coloscopy, or endoscopy of the colon. Coloscopy is usually made if the patient has a history of polyps, or if the physician suspects some colonic disease due to symptoms such as rectal bleeding, abdominal pain or change of bowel habits. If malignant growth is suspected, bi-

opsy samples are always collected during coloscopy for histopathological classification. Polyps are frequently found during endoscopic examination of patients. Polyps are tumourous masses inside the colon wall that protrude into the lumen of the colon (Fig. 14). They can either sit on stalks or be more flat. Adenomatous polyps are neoplastic, i.e. they harbour some malignant potential and may develop into carcinomas if left untreated. Other polyps, however, are nonneoplastic and do not have malignant potential. Hyperplastic and metaplastic polyps belong to this category. Nonneoplastic polyps represent approximately 90 % of all colorectal polyps, and it is estimated that they can be found in more than half of all persons above the age of 60. There is strong evidence that most invasive colorectal adenocarcinomas arise in adenomatous polyps. It takes an adenomatous polyp approximately 10 years to progress to an invasive stage.[95] It is sometimes difficult to distinguish between nonneoplastic and neoplastic polyps by conventional endoscopy, especially if they are small and flat.[96] Therefore, polyps found during coloscopy are usually removed and subjected to histologic evaluation. It would be interesting with a method assisting the examining physician to classify polyps during the endoscopic procedure. Fluorescence might provide the necessary information.
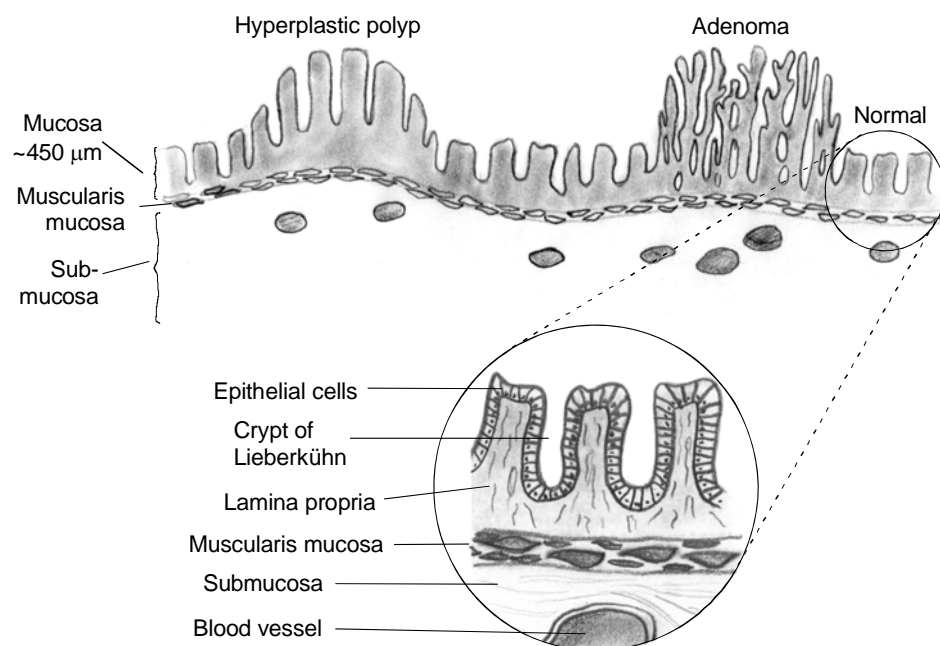

Fig. 14 Schematic drawing of colon wall showing normal mucosa, a hyperplastic and an adenomatous lesion.

In Papers VI and VII the feasibility of using laser-induced fluorescence to distinguish different types of colon polyps was evaluated. These papers present results from clinical measurements performed *in vivo* in the colorectal region of patients. The patients were examined by diagnostic coloscopy, where an endoscopic instrument (colonoscope) is used to view the mucosa inside the colon. An optical fibre guided the excitation light from the light source to the tissue, collected the tissue fluorescence and guided it back to the detection part of the fluorosensor (Fig. 15).
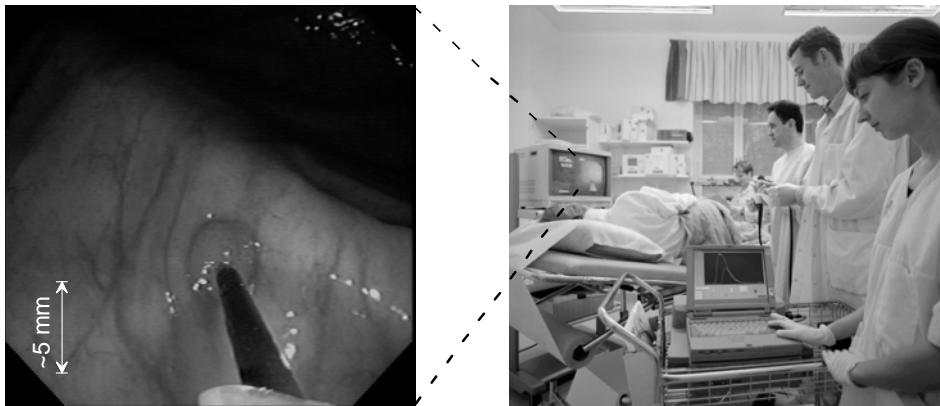

Fig. 15 The author and colleagues measuring laser-induced fluorescence at the Karolinska Hospital. The inset shows the endoscopic view of the optical fibre in contact with a polyp.

Fig. 15 shows the clinical setting for fluorescence measurements in the colon, performed at the Karolinska Hospital. The fluorosensor, in the bottom right of the right picture, is the size of a briefcase and could easily be moved around the clinic.[97,98] The tip of the colonoscope used is equipped with a video camera, and the operating physician navigates the flexible instrument in through the entire colon and examines the tissue mucosa on a TV screen. To the left in Fig. 15, the image on the monitor is enlarged, showing how the optical fibre is in contact with a small polyp for fluorescence measurement. The results from these studies show that laser-induced fluorescence might improve the sensitivity and specificity of endoscopic characterization of polyps. This is also discussed in more detail later in this chapter.

4.1.2 Larynx

The larynx is situated in the upper airways, between the pharynx, or throat, and the trachea. Its primary functions are phonation, airway protection during swallowing and coughing. It houses the vocal and ventricular folds, also called the true and false vocal cords. The vocal folds are two small strong bands of elastic tissue

stretched across the airway, which vibrate and make sounds as air passes. Fig. 16 shows an endoscopic view of the vocal folds. They are covered by a stratified squamous epithelium, composed of several cell layers with flattened cells in the superficial layers (Fig. 17). The total thickness of the epithelium is approximately 200 μm. Squamous cell carcinoma in the larynx is the most common malignancy in the head and neck region, but its occurrence in nonsmokers is very rare.[99] A long-lasting hoarseness is the most common symptom.
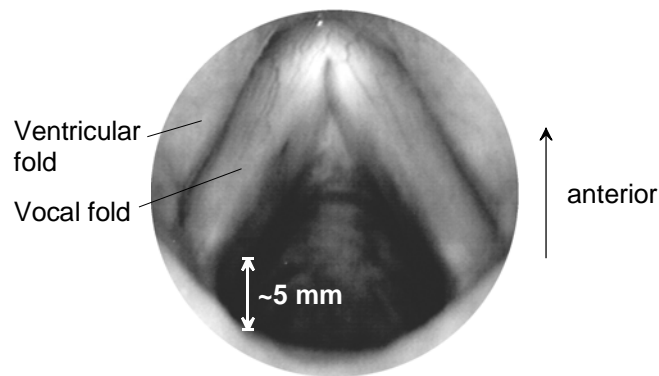

Fig. 16 Endoscopic view of the larynx, showing the vocal and ventricular folds.

In dysplastic epithelium, the layered structure is partly lost and the cell nuclei become irregular and enlarged. It starts in the deepest lying cell layers, and gets more superficial with increasing grade of dysplasia. In carcinoma *in situ* (CIS), the layered structure is totally lost, and the dysplastic cells are present throughout the epithelium. However, the basement membrane is still intact and prevents access to vascular channels, and hence metastasis.

The larynx can be examined by laryngeal endoscopy, laryngoscopy, often in combination with microscopic equipment.[100] For the optimal treatment of laryngeal malignancies, the early detection and accurate localization are important. The distinction between dysplasia, CIS and invasive carcinoma is also important, since the therapeutic procedure depends on the stage of malignant transformation. Sometimes there can be a superficial keratin layer on the epithelium. The whitish keratin can hide dysplastic tissue underneath and makes examination difficult. At surgical removal of a lesion it is important to know the tumour extension. The surgery has to be radical, but the removal of healthy surrounding tissue should be avoided in order to keep as much function as possible of this small and delicate organ. Attempts to use fluorescence to discover premalignant or malignant lesions, determine their progression and delineate their borders have been made. In Papers VIII

and IX, fluorescence measurements of the vocal and ventricular folds are presented. Fibre-based fluorosensor systems are well suited for measurements in real-time during laryngoscopical examination.
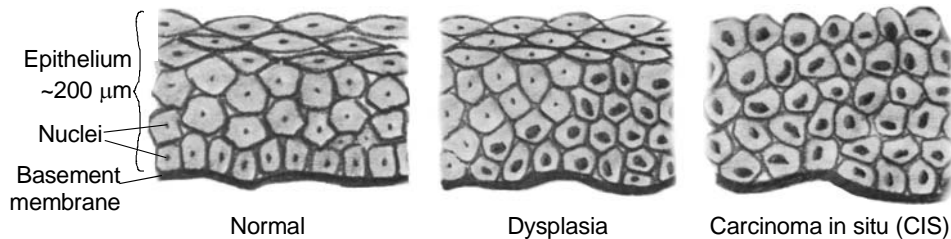

Fig. 17 Stratified (layered) squamous epithelium of the vocal folds. From left to right normal epithelium, dysplastic epithelium and carcinoma in situ.

4.2 The physical basis of fluorescence

Tissue fluorescence involves the absorption of a photon by a molecule and the subsequent emission of a fluorescence photon. Absorbing molecules, previously referred to as chromophores, that release their excess energy by emitting fluorescence light are usually called fluorophores. The electronic states of a molecule can be described by a Jablonski diagram (Fig. 18). If the electron spins are paired, the energy level is a singlet state, denoted S, while unpaired electron spins will give a triplet state, T. The ground state of most molecules is a singlet state. The electronic states of molecules are divided in vibrational states, which in turn are divided in rotational sublevels. If an incoming photon has an energy that corresponds to the energy difference between an excited state and the ground state of the molecule, it can be absorbed. The absorption bands of most molecules in tissue are very broad. This is due to the many rotational levels, partially overlapping each other due to the strong interaction between nearby molecules causing a varying external field for each molecule. The photon energy will thereby be used for excitation of the molecule to the higher energy band. Fig. 18 shows an excitation from the ground state to the S_1 band. The molecule rapidly relaxes down to the lower level of S_1 by internal conversion, which is a nonradiative process. The deexcitation to the S_0 band can also occur through internal conversion. Alternatively, it can result in the emission of a fluorescence photon. The relaxation can take place to any vibrational level in S_0, and hence the total fluorescence from the molecule will not be a sharp peak at one distinct wavelength, but a broader distribution. Since some energy was lost in the nonradiative relaxations, the
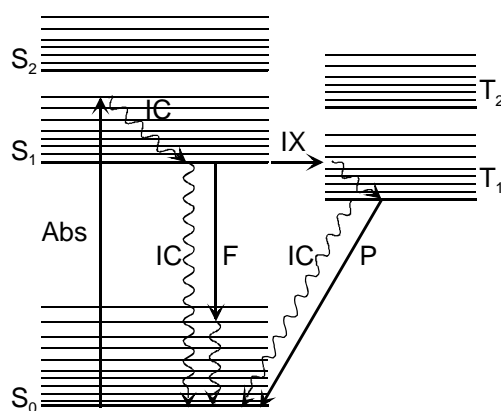
Fig. 18 Jablonski diagram showing absorption of a photon and some of the possible relaxation processes. IC, internal conversion; F, fluorescence; IX, intersystem crossing; P, phosphorescence.

fluorescence will have a lower energy and thus a longer wavelength than the incoming excitation photon. From the excited state S_1, a transition can also take place to a triplet state, even though this is a spin-forbidden transition. Transitions from the triplet state back to S_0 are also spin-forbidden, and it will take a relatively long time before the molecule relaxes. Again, the relaxation can occur through internal conversion or by emission of a photon. This process is called phosphorescence and has a lifetime in the microsecond to second range, while fluorescence lifetimes are in the nanosecond range.

Fluorescence from tissue can be studied in different ways. Excitation spectra are obtained by varying the excitation wavelength while detecting at a fixed wavelength. If the excitation wavelength is constant and the fluorescence is detected at several wavelengths, emission spectra are obtained. Excitation–emission matrices (EEMs) can be produced when repeating measurements of the emission spectra for different excitation wavelengths. Different studies have presented EEMs from normal and tumour tissue from various sites in the body.[101-103] These can be helpful in indicating the most appropriate wavelengths to use for clinical LIF studies. The fluorescence decay times can also be studied with time resolved measurements.[104-106] Different fluorophores have different decay times, and by fitting a sum of decay curves to experimental data, the fluorophores can be identified. In Paper X time-resolved and spectrally resolved imaging of skin lesions is performed. This is discussed in Chapter 4.6.2. The majority of the fluorescence work in this thesis deals, however, with emission spectra.

4.3 Autofluorescence

Under UV or blue light irradiation, several fluorophores in tissue will yield a broad fluorescence distribution in the visible wavelength region. This fluorescence is referred to as the autofluorescence, or endogenous fluorescence, as compared to the fluorescence due to some exogenous dye, which will be discussed in the next chapter. The spectra are also influenced by the optical properties of the tissue. Strong absorbers, such as haemoglobin, may decrease the overall intensity of the fluorescence spectrum, without changing its shape, by absorbing the excitation light.[15] Haemoglobin can also absorb fluorescence light at certain wavelengths and thus change the appearance of the fluorescence spectrum, creating false dips and peaks. Naturally, the shape of the spectrum also depends on the excitation wavelength, since this will determine what energy transitions in the fluorophores are possible. Most often, excitation in the ultraviolet or blue wavelength region is used for LIF studies of tissue. The fluorescence spectra are very complex, and the contributions from the different fluorophores can usually not be separated. Fig. 19 shows the fluorescence spectra from some important tissue fluorophores under 337 nm excitation. Collagen, elastin, NADH, tryptophan, porphyrins and FAD are known to fluoresce strongly.[14-16]
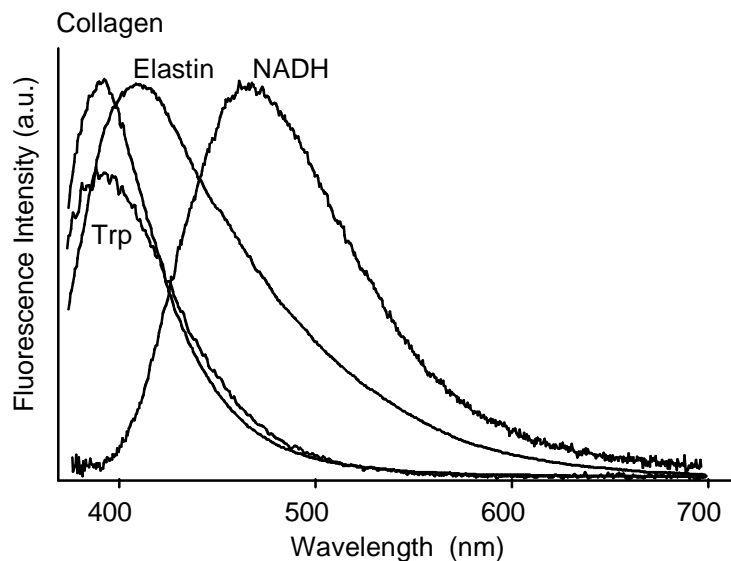

Fig. 19 Fluorescence spectra from some tissue fluorophores following 337 nm excitation.[107,108] Please note some of the chromophores have other emission peaks when excited at other wavelengths.

4.3.1 Collagen and elastin

Collagen and elastin, which are fibrous proteins abundant in connective tissues, contribute significantly to the fluorescence signal of tissues following 337 nm excitation. There are several different types of collagen in the body, normally denoted by different numbers, which have slightly different fluorescence maxima. Collagen I is abundant in skin, ligaments, internal organs etc., and accounts for 90 % of the body collagen.[109] It has an excitation maximum at 340 nm, and a corresponding fluorescence peak at 395.[107] Other fluorescence excitation/emission maxima of collagen I are at (270/395 nm) and (285/310 nm).[110] In the basement membrane of epithelial tissues, collagen IV is abundant. Elastin fluoresces at 410 nm when excited at 337 nm.[107,110]

4.3.2 NADH

NADH is the reduced form of nicotinamide adenine dinucleotide, and plays an important role in the metabolism of the cell. Approximately 80 % of the NADH is situated in the mitochondria of the cells, while the rest is in the cyto-sol.[111] NADH has an excitation/emission maximum at (350/460 nm), while its oxidized form NAD+ does not fluoresce if excited above 300 nm. At low oxygen levels, this balance is shifted towards NADH.[112] Hence, a higher metabolic rate due to for example an inflammatory reaction can lead to an increased NADH fluorescence.[60]

4.3.3 Other fluorophores

Tryptophan is an amino acid (subunit of proteins). It has an excitation/emission maximum at (275/350 nm) when in aqueous solution, and when excited at 337 nm it fluoresces at approximately 390 nm. There may be an increased amount of tryptophan in premalignant tissue as compared to normal tissue, but its contribution to tissue fluorescence when exciting at wavelengths above 300 nm is small. Other endogenous fluorophores include flavins,[16,113] lipofuscin,[114] and endogenous porphyrins.[18,115]

4.3.4 An example: colon lesions

Clinical measurements have been performed on many different tissue types.[92,101,116-118] The clinical objectives of fluorescence measurements in the colon are described in Chapter 4.1.1. Fig. 20 shows an example of the fluorescence, following 337 nm excitation with a N$_2$ laser, from normal, hyperplastic and adenomatous tissue *in vivo* in the colon.
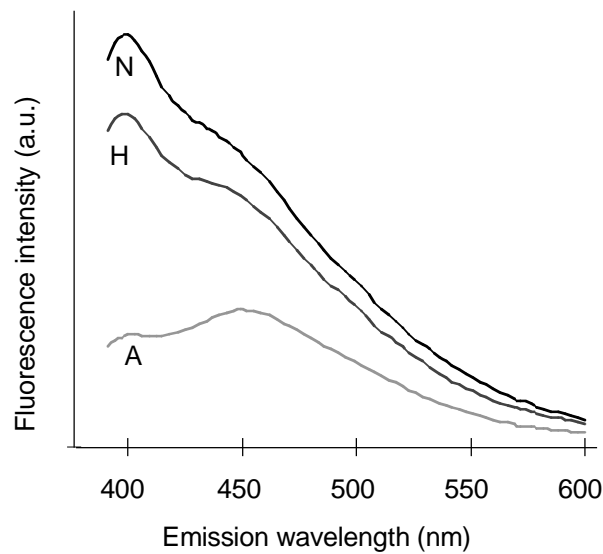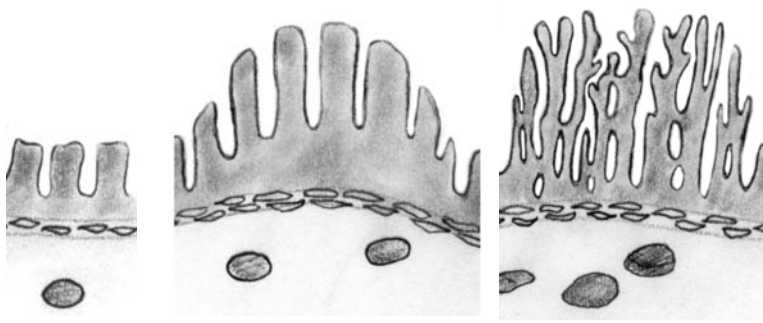
Fig. 20 Typical fluorescence spectra obtained in vivo from normal (N), hyperplastic (H) and adenomatous (A) colon mucosa; at 337 nm excitation.

It can be seen in the figure that the fluorescence from normal colonic mucosa has its highest peak around 390 nm, close to the fluorescence peak of collagen. Hyperplastic mucosa has a similar emission spectrum. However, in adenomatous tissue, the highest peak is at a higher wavelength, around 460 nm. Schomacker *et al.* suggested that this is because the epithelium is thicker and submucosal collagen signal decreases, i.e. that the difference is due to polyp morphology alone.[94] However, this does not explain the difference in spectral shape between hyperplastic and adenomatous polyps. Some other possible explanations can be seen in Fig. 21. Collagen is present both in the submucosa and in the lamina propria. In adenomatous tissue, the crypts tend to enlarge and the epithelial cells proliferate more, which crowds out the lamina propria, which is a source of collagen fluorescence in hyperplastic as well as in normal colon mucosa.[119] Römer *et al.* observed by fluorescence microscopy that fewer fluorescent collagen fibres were present in the lamina propria of colonic adenomas as compared to normal colon.[120] They also saw fluorescence from the cytoplasm of dysplastic epithelial cells, which increased in intensity with increasing grade of dysplasia. Zonios *et al.* reported that dysplastic epithelial cells fluoresce near 440 nm with an additional component above 600 nm, using 370 nm excitation. This fluorescence, in combination with a decreased collagen signal, could explain the differences in spectral shape in adenomatous as compared to normal and hyperplastic colon tissue. Fiarman *et al.* detected epithelial cell fluorescence also from hyperplastic tissue,[121] while Da Costa *et al.* did not.[122] It is not

yet established which fluorophore emits this fluorescence. The emission wavelength corresponds quite well to NADH. As discussed above, cells with a high metabolic rate can show an increase in NADH fluorescence, so this is one possible candidate. Other theories of the origin of this epithelial fluorescence include lipofuscin[122] and incomplete haem synthesis.[119] Another difference between the spectra is an overall intensity reduction in the adenomas. This could be due to lower abundance of the fluorophores, but probably also to an increased haemoglobin content in the adenomas, giving an increased overall absorption. Schomacker *et al.* have reported a successive increase in the relative contribution to the fluorescence signal from NADH going from normal to hyperplastic to adenomatous tissue.[94] Correspondingly, the relative contribution from collagen decreases going from normal to hyperplasia to adenoma.

	NORMAL	HYPERPLASIA	ADENOMA
Epithelial cells	no fluorescence	no fluorescence?	fluorescence (NADH?)
Lamina propria	collagen signal	increased collagen signal	decreased collagen signal
Submucosa	collagen signal	decreased collagen signal	decreased collagen signal
			increased haemoglobin absorption

Fig. 21 Possible reasons for the differences in fluorescence, compared to normal mucosa, in colonic lesions as measured from the surface.

4.4 Fluorescent tumour marking substances

In some cases, the ability to detect lesions by LIF can be further enhanced by the use of fluorescent tumour markers. These are substances that can be given to the patient before examination, usually by intravenous injection or oral administration. They are accumulated in malignant or pre-cancerous lesions to a higher degree than in healthy tissue, and their fluorescence will add features to recorded fluorescence spectra. This signal will contribute to the difference in fluorescence spectra recorded from diseased and normal tissue and thus be of help in demarcating the diseased lesions from the normal surrounding tissue. Many of these substances can also be used as photosensitizers for photodynamic therapy (PDT) of lesions. In this case the substance doses are usually higher than needed for fluorescence diagnostic purposes. PDT will be discussed briefly in Chapter 4.7.

Haematoporphyrin derivative (HpD) is a well-known tumour marker that has been used for fluorescence diagnostics and PDT in many studies. It is a mixture of different kinds of porphyrins. Porphyrins are similar in structure to the haem molecule of haemoglobin. They have a strong absorption band, the Soret band, near 400 nm and several smaller absorption bands, Q bands, at 480-650 nm.[123] HpD has characteristic fluorescence peaks in the red at about 630 and 690 nm. The main disadvantages of HpD are the long time required between administration and selective uptake in malignant tissue (24-48 h), and that the selectivity to malignant tissue is only about 2-3/1. Furthermore, the rate of clearance from the body is rather slow, and following an injection of a normal dose of HpD the patient will remain sensitive to sunlight for several weeks.[124] It is also a rather unstable compound, and it is difficult to purify. Therefore the evaluation of other tumour markers and photosensitizers has been a topic of intense research.

One useful substance is δ-aminolevulinic acid (ALA), which was used in Papers VI-X. It is a nonfluorescing substance that is naturally abundant in the cells, as a precursor to haem. The production of haem in the cell is a cycle in many steps that is regulated by several feedback functions. If an excessive amount of ALA is introduced to the system, this will result in a build-up of the fluorescent compound protoporphyrin IX (PpIX)[125]. PpIX accumulates in this way selectively in some tumour cells,[126] due to a different enzyme contents,[127] and, in the case of topical application of ALA on skin malignancies, due to an increased skin permeability in tumour tissue. The metabolic pathways of ALA have been of research interest since long.[128,129] PpIX, and not ALA, is the actual tumour marker. It is the immediate precursor to haem, and it is a strong fluorophore, similar to the monomeric compounds in HpD. When excited with light at 405 nm it will show a dual-peaked fluorescence in the red at approximately 635 and 700 nm (Fig. 22). Clinically, ALA can be given to the patients orally, intravenously or topically.[130,131] Compared to many other tumour marking substances, ALA has a fast clearance rate from the

body. The enzyme system regulating the haem cycle in the tumour cells is different from that in healthy cells, and PpIX will be more rapidly produced in tumour cells. Thus, the proper timing for fluorescence measurements is important.[125,132] In Papers VI-X, the ALA was given orally in low doses (5 or 7.5 mg per kg body weight). A study measuring the PpIX fluorescence in skin and in the mucosa of the ear-nose-throat region at different times after oral administration of ALA at similar substance doses, shows that maximal fluorescence occurs at 3-4 hours after administration.[133]

Fig. 22 shows average fluorescence spectra from laryngeal mucosa measured *in vivo* a few hours after oral administration of ALA. Light of 405 nm wavelength was used. A decrease in autofluorescence from premalignant as compared to healthy tissue can be seen, as in the case of 337 nm excitation above. The peaks at 635 nm are due to PpIX. The highest PpIX peak is seen in the premalignant tissue.
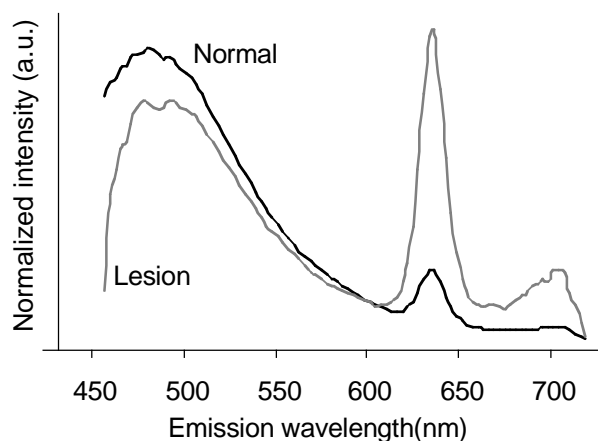
Fig. 22 Typical average fluorescence spectra obtained in vivo from normal tissue and premalignant lesion on vocal folds; using 405 nm excitation in patients who were given ALA prior to the examination.

In the colon, adenomatous colon polyps can be distinguished from normal using ALA and 405 nm excitation (Paper VI). However, there seems to be poor selectivity of ALA in adenomas as compared to hyperplastic tissue. This is discussed further in Paper VII.

4.5 Point monitoring

The diagnosis of tissue by histopathology involves removing a small tissue sample, a biopsy. When optical biopsy using the fluorescence technique is discussed, it usually means fluorescence point measurements, as opposed to fluorescence imaging, on the tissue. Point measurements involve the collection of spectroscopic information in a small tissue area using an optical fibre probe to guide the excitation to the tissue and to collect the tissue fluorescence. An optical multi-channel analyser (OMA) system for such measurements is shown in Fig. 23. An example of the measurement situation can be seen in Fig. 15, while typical spectra recorded are presented in Fig. 20 and Fig. 22. The fluorescence light is very weak compared to the excitation light, and therefore the detector system must be sensitive and the ambient background light must usually be efficiently suppressed. This can be achieved by using a pulsed laser and a gated detector. The laser light is focussed onto the end of an optical fibre. After each excitation pulse, fluorescence is emitted from the tissue. In our system it is collected by the same fibre, split off from the excitation path by a dichroic mirror and filtered to remove all excitation light. It is then focussed onto the slit of a polychromator, which splits up the light into its spectral components. A CCD camera images the spectrum, and sends it to a computer. The optical fibre is roughly 1 mm in diameter, and can easily be inserted into the biopsy channel of an endoscope. In this way, LIF point monitoring can be used together with endoscopy to examine many hollow organs in the body, such as the vocal folds, the colon, the bronchi and the urinary bladder. It can also be used per-operatively.
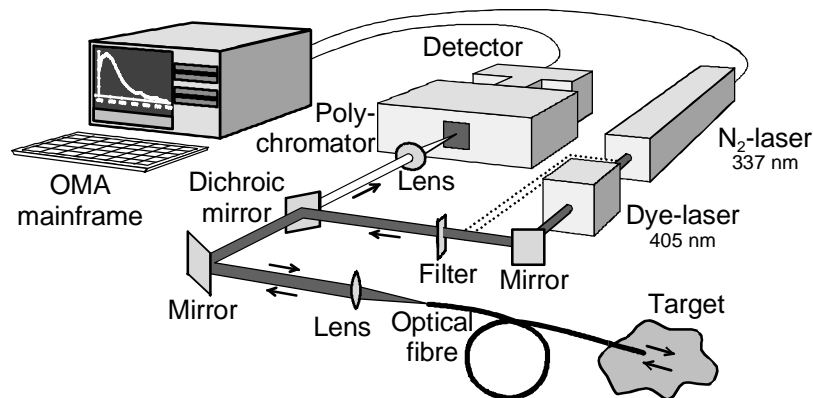

Fig. 23 Schematic drawing of OMA used for point measurements of fluorescence. From af Klinteberg et al.[134]

4.6 Imaging

The point monitoring technique relies on the skill of the physician in finding suspicious areas, just as histopathology does. Some lesions, for example the flat adenoma that can arise in the colonic mucosa, are often difficult to discern even for the trained eye. In these cases an imaging system, which could work in conjunction with normal endoscopy, would be of great help.

4.6.1 Spectral imaging

In point monitoring the fluorescence emission at all wavelengths is measured in one point. It is difficult to acquire all this information for each pixel in an image. It would also be very memory consuming. In fluorescence imaging the emission at one or a few wavelengths only are thus usually measured. This or these wavelengths have to be chosen optimally for each application. The results from spectroscopic point measurement studies are important for this selection. A multi-colour imaging system developed in Lund was used in Paper X.[135-137] This system divides the fluorescence light by beam-splitting optics into four images, which are spatially identical but filtered in separate wavelength bands. The images are detected on an intensified CCD camera, which is gated to suppress background light. Computer processing of the images yields a fluorescence image with optimized contrast between normal and diseased tissue. Normally, three images are used in the contrast function, which is on the form

$$F_c = \frac{A - k_1 D}{k_2 B}.$$
(32)

Here, A is the fluorescence detected in the red wavelength region, usually related to a fluorescent tumour marker. D is the fluorescence in a green-yellow wavelength band, which is multiplied by a constant and subtracted from the fluorescence in A to yield the pure tumour marker signal without any influence of tissue autofluorescence. The fluorescence intensity B originates from the autofluorescence around 470 nm. This contrast function, which yields high values for malignant tissues containing large amounts of tumour marking substance, is calculated in each pixel to create a new fluorescence image. If a video endoscope is used, the false-colour coded fluorescence image can be superimposed on the normal endoscope image in real-time, marking suspicious areas. This system has been used in a variety of clinical specialities, using different fluorescent tumour markers.[138] Other techniques than the one mentioned above have also been used in fluorescence imaging systems.[92,139]

Evidently, it is very important to choose good detection wavelengths and evaluation criteria to optimize the performance of the imaging system. In order to do so, studying spectra from point-monitoring measurements can be of great help, as

mentioned above. However, one must be careful when applying point-monitoring results to imaging, since the measurement geometries are different. In point monitoring, the fibre probe is held in gentle contact with the tissue. The fluorescence is collected with the same fibre, and thus the light transport in the tissue is very short. In the imaging case, the delivery and collection fibre bundles are kept away from the tissue. Both the excitation and fluorescence light will be scattered to a greater extent in the tissue, and light absorption, e.g. by haemoglobin, will alter the spectral shape. Examples of fluorescence spectra for different geometries of illumination and detection are shown in Fig. 24. All three spectra were recorded from exactly the same location of the tissue, using the same excitation and detection system. The only difference is the measurement geometry. These measurements were performed with 405 nm excitation. Fig. 24a shows the point monitoring geometry used for example in Papers VI-IX, with the same fibre used for both excitation and detection, and the fibre held in contact with the tissue surface. It can be seen in Fig. 24b that when a broad illumination is used and the detection fibre is kept in contact with the tissue, the light reaching the fibre has had to travel a certain distance in the tissue. Thus, the haemoglobin absorption decreases the autofluorescence intensity and creates a dip in the fluorescence spectrum at approximately 580 nm, corresponding to an absorption band of arterial blood. If a broad illumination is used and the detection fibre is kept above the tissue, both long and short photon paths will be detected, and the haemoglobin absorption of the fluorescence light is not as strong (Fig. 24c). Similar results have been shown by Keijzer *et al.*, who made measurements on human aorta in different geometries.[140]
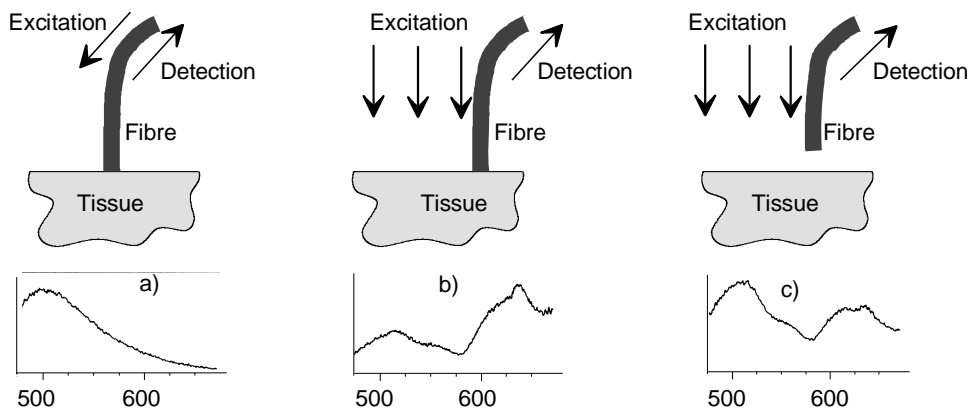

Fig. 24 The influence of different measurement geometries on fluorescence spectra.

4.6.2 Time-resolved imaging

Measurement of fluorescence lifetimes can provide additional information about the tissue chromophores and their environment. Because several tissue chromophores contribute to the fluorescence, a fluorescence lifetime measurement yields a curve that is the sum of all decays. A fit to three exponential decays is often performed.[141]

Fluorescent tumour markers usually have longer fluorescence lifetimes than the natural chromophores in tissue. Cubeddu *et al.* have developed an instrument for fluorescence lifetime imaging to detect fluorescent tumour marker.[142] This system was used in Paper X. A pulsed dye laser produces pulsed excitation at 405 nm. The autofluorescence is suppressed by filtering the signal, and a time-gated detection system acquires images at different times after the excitation pulse. A mono-exponential decay function is fit to the results, yielding a false colour coded image of the fluorescence lifetimes.

4.7 Photodynamic therapy

The use of tumour markers or photosensitizers also serves another purpose. Photosensitizers are essential in photodynamic therapy (PDT), which is a nonthermal technique used mainly for the treatment of malignant tumours where the sensitized cells are selectively killed with minimal or no damage of the surrounding healthy tissue.[124,130,143,144] The photodynamic reaction is dependent on the presence of photosensitizer and oxygen, and activated by light irradiation. The absorption of light by the photosensitizer will cause the transformation of oxygen from its ground state to its singlet state. Singlet oxygen acts as a very aggressive oxidant on many molecules in the cell, and the cell is killed. To ensure that only malignant cells are killed in this process, it is essential to use a photosensitizer that has a high selectivity for tumours. Light dosimetry can also be an important factor. The selective killing of malignant cells is of course a great advantage. Conventional treatment modalities such as radiation therapy, utilising ionising radiation, and chemotherapy have poor selectivity. They rely on that the malignant tissue has poorer recovery after treatment and on accurate dosimetry calculations in order to spare as much healthy tissue as possible and still destroy the malignancy. PDT has been performed e.g. on nonmelanoma skin tumours[131,145] and on the surface of hollow organs[146]. It is an especially interesting alternative in sensitive areas or where surgery can be cumbersome, e.g. on the vocal folds or on the skin close to the eye. The cosmetic result is often superior to that of surgery, since there is little scar formation.[131]

A high light absorption by the photosensitizer is important for the therapeutic result. Porphyrins, for example, have several absorption bands in the visible wavelength region, the strongest being the Soret band around 400 nm, which is used for

fluorescence studies. Still, longer wavelengths are preferable for PDT, usually around 630 nm. This is due to the larger penetration depth of light at this wavelength, as discussed in Chapter 2, allowing the treatment of thicker lesions. However, the shallow treatment depth is still one of the main disadvantages of PDT. Insterstitial delivery systems have been developed, allowing treatment of larger tumours by inserting optical fibres into the tumour mass and irradiating from within.[147,148]

Another disadvantage of PDT is that the photosensitizer dose has to be higher for PDT treatment than for LIF measurements, and the patients may experience the side-effect of skin photosensitivity. This means that they should stay out of the sun for days up to weeks.

Chapter 5
Analysis of fluorescence data

To classify fluorescence emission spectra, e.g. as diseased or healthy, some evaluation criterion must be chosen. This is a challenging task, given the complexity of the tissue, with several fluorescent biomolecules as well as absorbing (nonfluorescent) and scattering compounds. Each of these parameters normally shows variation between individuals and location. The variation between individuals is often large. The abundance of both the endogenous fluorophores and the exogenous fluorescent tumour marker, if one is used, can vary considerably. If the variations in normal tissues are too large, there can be an overlap with spectra measured on diseased tissues, and classification can be difficult. In these cases, it is often better to compare every measurement with a normal measurement from the same patient (Paper VIII).[149] For example, in patients given ALA the concentration of PpIX is usually higher in malignant tissue than in normal tissue in the same patient. However, there can be an offset, so that the normal porphyrin signal in one patient is comparable to the signal from a malignancy in another patient. This effect can be more easily handled in fluorescence imaging than in the point spectroscopy approach, as both malignant and normal tissue can be captured in the same image.

The existing techniques for tissue classification based on fluorescence data can roughly be divided into two categories; modelling and statistical methods. In the modelling approach the effects from intrinsic tissue fluorescence and light attenuation due to other tissue chromophores are separated. This can be done by proper modelling of the light transport in tissue. The modelling approach has the advantage that data obtained using different measurement methods and geometries can be compared, as the effect of light propagation is modelled. The statistical approach, on the other hand, does not require any such knowledge, but also lacks the advantage of transportability. Any changes in the recording procedure may require that the system must be retrained. This thesis only considers statistical methods in the evaluation of fluorescence data. In this chapter, a brief outline of the modelling approach is however given, while the multivariate methods are described in more

detail. In Paper IX, some different multivariate analysis methods have been compared.

5.1 Fluorescence modelling

Fluorescence modelling is an attractive method in that it yields information about the underlying factors affecting the fluorescence signal. By measuring the tissue absorption and scattering characteristics, e.g., by some type of diffuse reflectance measurement, major tissue chromophores can be determined and their concentrations can be estimated. In this way the effects on the signal from light attenuation and geometry can be determined. Obviously, the signal will depend on the tissue optical properties at both the excitation and emission wavelengths. An illustrating example of how the optical properties of the examined tissue may alter the recorded fluorescence spectrum is haemoglobin reabsorption of the fluorescence emission, causing an apparent double peak instead of the intrinsic single fluorescence peak. It is also obvious from Fig. 24 that reabsorption of fluorescence is important for the recorded signal. If the important chromophores in the tissue and their optical properties at all wavelengths studied and also all fluorophores contributing to the fluorescence emission and their fluorescence properties are known, their concentration in the tissue can be obtained by modelling and the least-squares fitting method.[150] This technique has been used to decompose fluorescence spectra, for example from the colon,[94] the cervix,[151] and aorta.[152] A limitation to the modelling approach is that a precise knowledge of the measurement geometry is required so that the light transport can be modelled accurately. This might be difficult since tissue is a complex system, and modelling will always include simplifications.

A technique closely related to fluorescence modelling has been used by af Klinteberg *et al.* to evaluate fluorescence from basal cell carcinomas before and after PDT. Three principal spectral components were determined by subtracting averaged, scaled spectra measured at different times during the treatment process. These spectra corresponded to the pure spectra from autofluorescence, PpIX and photoproducts from PDT. A least-squares fit of each measured spectrum to the linear combination of the component spectra was performed. The course of lesion treatment was evaluated by studying the fluorescence contribution from each of the components.[153]

5.2 Multivariate statistical techniques

In the statistical approach, there are several different multivariate analysis methods that can be used for spectral evaluation, such as multivariate linear regression (MVLR), principal component analysis (PCA), principal component regression (PCR) and partial least squares (PLS).[154,155] MVLR, used in Paper VI, is the most

frequently used multivariate method for tissue fluorescence spectra,[94,117,156-159] but principal component analysis has also been used.[160,161]

5.2.1   Background

To make the classification algorithm simple, the fluorescence intensities at a limited number of wavelengths in the spectrum are most often extracted. It is then important to choose the wavelengths where the lesion-to-normal contrast is as large as possible. An example of one of the simpler algorithms successfully used for this purpose is the dimensionless ratio of two fluorescence intensities.[12,116] This approach is very useful in fluorescence imaging, when it is only possible to detect a few emission wavelengths with a not too complex detection system. When ALA is used as a fluorescent marker, one can for example divide the fluorescence near the PpIX peak, which is higher in malignant tissue, with the autofluorescence, that is lower in malignancies, and in this way achieve a higher tumour demarcation. In addition, the sensitivity to variations in signal strength due to geometry or system performance is eliminated as a dimensionless quantity is used. This technique is employed in the fluorescence imaging system described in Chapter 4.6 (Paper X). When evaluating fluorescence ratios it is often good to choose two wavelengths where the influence from blood absorption is equally strong, so that this effect is cancelled out.[118,162]

Even though the ratio method works well in many cases, it requires a qualified guess of what wavelengths to use. In addition, there may be information hidden in the spectra that is not exploited in this way. To utilize more of the available and relevant spectral information, more sophisticated evaluation techniques are needed. Multivariate methods are used in various scientific fields for the analysis of experimental data and for optimal extraction of information.

5.2.2   The principles of multivariate methods

The fluorescence data can be represented as a matrix called X (Fig. 25). Each column vector in X represents one measured variable, in this case the fluorescence intensities in different spots at one certain wavelength. Each row vector corresponds to one observation, i.e., a fluorescence spectrum. The gold standard, i.e., the reference method whose results we want to predict, is the histopathological characterization of biopsy samples. These diagnoses are classified into groups, converted to discrete numbers and stored in a column vector y. X and y can be seen as the independent and dependent variables of the problem, respectively. The multivariate methods, except for MVLR, can be employed using full spectra. Hence, it is not necessary to simplify the data matrix X by selecting only a few of the fluorescence wavelengths for the analysis. The subset of multivariate approaches that are especially suitable for handling data with a large number of variables are often called *chemometric* techniques. As the name indicates, these methods

were first developed for the evaluation data from modern methods in analytical chemistry, such as spectroscopic and chromatographic methods.

Basically, multivariate analysis is used to transform measurements X into informative results, e.g. separating groups of data or creating a model for prediction of an interesting variable y. The different multivariate methods create slightly different models for this purpose, as described below. They have in common that the information in X is reduced to a simpler form. The resulting model can be used to predict the y values, i.e. the tissue pathologies, from measured spectra, provided these measurements were performed in a similar manner and hence can be considered as belonging to the same statistical population of spectra. Imagine, for example, a crude comparison with our own vision. The spectral information we receive as we look at for example the clear sky is interpreted, based on a previous "calibration", in our brain and simplified to meaningful, compressed information telling us it is blue. In the same way, the spectral information from a tissue fluorescence measurement can be interpreted, based on a previous multivariate calibration, as either diseased or healthy.
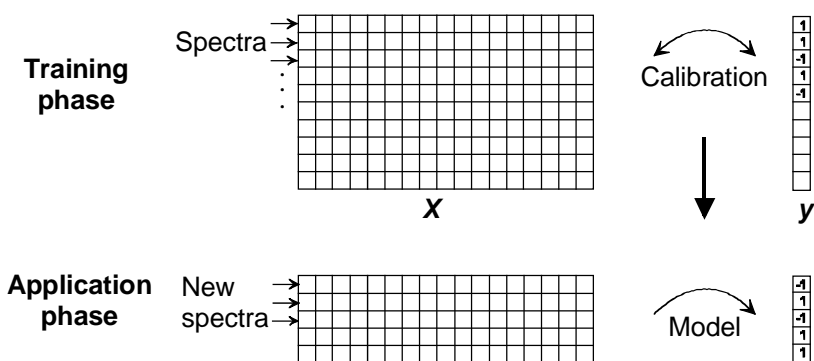

Fig. 25 Schematic view of calibration and prediction using a multivariate method. In the upper part, the spectra in X together with the known histopathologies in y are used for calibration, yielding a model. The model can be applied to new spectra recorded under the same conditions for prediction of tissue pathology (lower part).

In this thesis, multivariate methods have been used to detect differences in spectral shape rather than intensity. Normalized spectra have therefore been used.

Usually, the results are evaluated in terms of the obtained *sensitivity* and *specificity*. Sensitivity denotes the proportion of positives that are correctly classified by the method, while the specificity is the percentage of negatives that are correctly identified by the method. *Positives* and *negatives* are terms referring to the presence or ab-

sence of a condition, respectively. In the work presented here a positive is usually an abnormal pathology, such as a malignancy, as determined by histopathological examination. Thus, we are comparing our results to those obtained by the gold standard, histopathology, which in itself is a subjective method with occasional disagreement in the opinions of different pathologists.[93,94]

5.2.3 Validation

As mentioned above, multivariate calibration extracts the information of interest and thereby reduces the information in X. More specifically, the calibration transforms X into a new coordinate system with fewer dimensions. When performing the calibration, we have to decide on its level of complexity, i.e. how much should be included in the model and how much should be left out. The residual is the part of X that has not been included in the model. Optimally, the residual consists of noise or irrelevant information only. To avoid overfitting or underfitting of the model, and to study how well it will work for new data, validation is necessary. Validation is a phase, not shown in Fig. 25, in between the training and application phases. It produces a measure of the prediction error, telling how large an error we can expect when using the model for prediction of new data in the future. *RMSEP* (root mean square error of prediction) is a measurement of the prediction error in *y*. It is defined as the square root of the average of the squared differences between predicted and measured *y* values of the validation objects,

$$RMSEP = \sqrt{\frac{\sum_{i=1}^{n} (\hat{y}_i - y_i)^2}{n}}. \tag{34}$$

RMSEP is given in the original units of *y*. It is essential that the data used for calibration are representative for the data we want to predict. Thus, if there is an instrumental drift or other measurement variations over time, an old calibration model may give unexpected results and recalibration is necessary.

The most common validation methods are outlined below. All these can be used for either of the multivariate analysis methods.

Test set

The best way to validate the model is to use separate calibration and test sets. The measured spectra are then divided in two groups, where one is used for calibration and the other for validation only. The disadvantage with this method is that a large data set is needed.

Cross validation

In cross validation, part of the data set is used as a test set while the model is based on the rest of the data. Then this is repeated, leaving out another part, and so on.

The mean error for all these models is used as a total error. Note that the actual model is still based on all samples at the same time; the above mentioned routine is just used for validation to estimate the prediction error. *Full cross validation* means that one sample is left out of the model each time and used for testing. In *segmented cross validation* the samples are divided into groups and one group is left out each time. The disadvantage with cross validation is that the same samples influence both the model and the error estimate. Still, it is the best alternative for validation when there is not enough data for a separate test set.

Leverage correction

Leverage correction means that the error estimate is based on the residuals for the samples in the calibration set, and on how close to the model they are. The leverage is the effect of an object on the model, depending on how far it is from the model centre. An extreme sample, far from the model centre, has a large influence on the model and a large leverage. This sample also has a larger influence on the error estimate in leverage correction. A sample that is more typical is downweighted in the leverage correction method. This method is quick, but it underestimates the error. Therefore it is suitable mainly to obtain a rough estimate in the initial modelling stages.

Note that the actual model is the same regardless of whether leverage correction or cross validation is used. Only the estimated prediction error is affected by the validation method.

5.2.4 Multivariate linear regression

Multivariate linear regression (MVLR) is commonly used for tissue fluorescence evaluation (Paper VI).[94,117,157-159] It is a statistical method where the intensities at some chosen wavelengths are extracted and a predicted y value is given by a linear combination of these intensities

$$y = Xb + f, \tag{35}$$

where f is the residual, which should be as small as possible. The regression coefficients in b can be determined by least-square estimation to

$$\hat{b} = (X^T X)^{-1} X^T y. \tag{36}$$

The regression can be calculated stepwise, i.e. the variables (intensities at given emission wavelengths) are added or deleted at each step of the model build-up, depending on how significant their contributions to the model are. The parameters of the regression can be set to define how significant a wavelength must be in order to be included in the model. If the parameters are very strict, one can create a model that employs data from just one or two emission wavelengths.

MVLR is a method that is simple to implement and that can easily be used for predictions for new samples. However, the understanding of the physical reasons behind the formula derived is often limited. In addition, MVLR may fail if there are collinearities between variables in X or if there are more variables than samples. Therefore, when using MVLR for spectroscopic applications the full spectra cannot be used, but the fluorescence intensities at some well-chosen wavelengths have to be extracted.

5.2.5 Principal component analysis

Principal component analysis (PCA)[154,163] is another possible evaluation method for tissue classification. The principle of PCA is to find a way to describe X, taking into account as much as possible of the relevant variations in our spectra without including the variations that are only due to noise. In doing so, X is divided in a structure part and a noise part. Linear combinations of the original variables in X are now combined into so called principal components (PC:s), and the structure part of X is described in terms of these. If X consists of r rows and k columns, each observation can be represented as a point in a k-dimensional coordinate system, and in total there will be r such points. The principal components can be seen as directions in this k-dimensional space. The first principal component, PC1, is chosen as the direction along which the variance in X is the largest. PC2 is chosen as the next largest variance orthogonal to PC1, and so on. After a certain number of components, the variance is so small that the rest of the principal components can be considered as noise. The *loading vectors* or *loadings* are the representations of the principal components in the original variables. X can be described by the matrix equation

$$X = TP^T + E, \tag{37}$$

where P is a matrix containing the loadings, T is the score matrix, i.e. the projections of the observations down on each loading vector, and E is the residual (noise). This can be seen as a transform of X into a new coordinate system with fewer dimensions. The number of dimensions is equal to the number of principal components included in the model. The loading matrix P can be seen as a transformation matrix between the original variable space and the space spanned by the principal components, and the scores in T are the coordinates of all samples in the new principal component space.

Principle component regression (PCR) is a similar method. First, PCA is made on the X-matrix according to Equation (37), and then the resulting T-matrix is used for MVLR. When using PCR, collinear data are not a problem. However, one disadvantage with PCR and PCA is that they do not take y into account in the selec-

tion of principal components. The principal components might thus describe some variations in X that are not correlated with y. Excluding these variations from the model might improve the prediction ability.

5.2.6 Partial least squares

While the principal components determined by PCA simply describe the largest variations in X, partial least squares (PLS) strives to find the components in X that correlate the most with y. By allowing the y data to intervene in the X decomposition, the impact of large but irrelevant spectral features in X is reduced. There are two different types of PLS: PLS1 is used when there is only one y variable, and PLS2 is used when Y is a matrix containing several variables.[155] The first PLS component is chosen as the direction in X that correlates the best with y. Note that the PLS component does not have to be equal to the principal component from PCA. The second PLS component is chosen in the same way, after subtracting the first principal component from X, etc. PLS may be the most complicated of the multivariate methods, but it is also the most powerful method to find the relationships between X and y. PLS is normally used for quantitative purposes, e.g., to determine concentrations of sample constituents, but has also proven useful for classification purposes, PLS discriminant analysis (PLS-DA).[164] For this purpose, y is given discrete values for the calibration, usually +1 and –1, depending on the class belonging (Papers VII and IX).

5.2.7 Logistic regression

Logistic regression is a popular method for medical statistical evaluation, since it assumes that the dependent variable (y) is discrete and binary. A logistic function logit(x) is an S-shaped curve going from 0 to 1 as x goes from -∞ to ∞ like the one shown in Fig. 26. In this case, the posterior probability P(y|T) should behave as a logistic function. P(y|T) is the probability that the dependent variable has a value y, given a test result T. How the fluorescence spectral shape can be incorporated into the test result T will be discussed below.
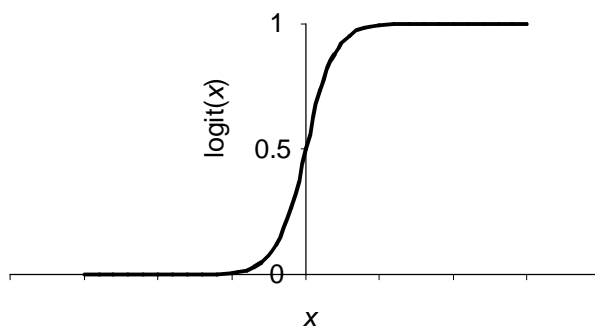

Fig. 26 Plot showing the S-shaped form of a logistic function.

The model used in Paper IX is based on Bayes' theorem. This is used to calculate the probability for a measured lesion to be diseased, given a certain test result. In the simplest case, with two diagnostic classes (disease/nondisease) and two possible outcomes of the test, Bayes' theorem is given by

$$P(N \mid -) = \frac{P(- \mid N)P(N)}{P(-)},$$
(38)

where P(N|-) is the probability that the tissue is normal, given a negative test result (-). P(-|N) is the conditional probability that a normal tissue has a negative test result, and P(N) is the prior probability that the tissue is normal. The test result in Equation (28) can be connected to the result from a fluorescence measurement. Ramanujam *et al.*[160] have used PCA for this purpose. Bayes theorem will then have the form

$$P(N \mid T) = \frac{P(T \mid N) \times P(N) \times C(L \mid N)}{P(T \mid N) \times P(N) \times C(L \mid N) + P(T \mid L) \times P(L) \times C(N \mid L)},$$
(39)

where P(N|T) is the posterior probability that the tissue is normal if its spectrum has the principal component scores T, and P(T|N) is the conditional probability that a normal tissue sample will have scores T. P(N) is the prior probability that the tissue is normal. The conditional probabilities are determined by fitting a normal or gamma probability density function to the scores for each principal component and each group (N and L). The costs of misclassifying a normal tissue as a lesion or vice versa are denoted C(L|N) and C(N|L), respectively. They can be varied for best sensitivity and specificity, as long as their sum is equal to one. The conditional probabilities for all principal components are multiplied to yield the conditional joint probability for each group. Logistic techniques can also be combined with PLS analysis (Paper IX).[165]

5.2.8 Other techniques

There are a number of other options for spectral evaluation available.[157,166] Vo-Dinh *et al.* obtained good results evaluating fluorescence spectra from the oesophagus by using differential normalized fluorescence (DNF). The mean average of a number of normalized fluorescence spectra from normal tissue was used as a baseline, which was subtracted from measured spectra. Combinations of peak intensities and curve slopes have also been used.[149]

In summary, the purpose of the multivariate fluorescence analysis discussed in this chapter is to allow the interpretation of fluorescence spectra to comprehensive information about tissue status. This could be implemented in diagnostic equipment to provide clinically useful information in almost real-time.

Acknowledgements

It has truly been a privilege to be a PhD student at the Atomic Physics Division and Lund University Medical Laser Centre, and having the possibility to work in the border zone between physics and medicine. I would like to express my gratitude to all the people who have made my work with this thesis easier, better and more fun.

First of all I would like to thank my supervisor, Dr. Stefan Andersson-Engels. He is not only helpful and amazingly patient as a supervisor, but also a good friend whom I have really enjoyed working and travelling with. I am also grateful for the nice collaboration with my other two supervisors, Dr. Katarina Svanberg and Prof. Sune Svanberg, who have taught me a lot about the fascinating worlds of medicine and physics. It has been a pleasure to work closely together with these people who with their skills, enthusiasm and hard work have built up a very strong lab with a friendly and informal atmosphere. Many graduate students and post-docs have also contributed to this atmosphere. I would especially like to thank Claes af Klinteberg, whom I have too often torn from his work to help me with mine, or just to kill some time over a cup of coffee. Christian Sturesson was a great office mate for four years. Sadly, our office space has deteriorated, in many ways, since he left. I am glad to have had Annika Enejder as a classmate, colleague and good friend these years. I have also enjoyed the nice collaboration with Ingrid Wang. In addition, I would like to thank the other past and present members of the medicine group and the rest of staff at the Atomic Physics Division for a stimulating collaboration.

The months I spent in the lab of Prof. Bruce Tromberg at the Beckman Laser Institute in Irvine, were among the absolute highlights of my time as a PhD student. Bruce has a highly contagious enthusiasm, and after just a short discussion with him on my arrival I had forgotten about the Californian sun and was really excited about spending the whole winter in his lab, sending light into a bucket of lard. He has a group of very nice people working for him, and I would like to thank them all for their hospitality and friendship. In particular I would like to thank those who have contributed in one way or the other to the work presented in this thesis; Tuan Pham, Josh Fishkin, Natasha Shah, and Andrew Berger.

I am happy to have had the opportunity to work with and get to know the research group of Prof. Rinaldo Cubbedu at Politecnico di Milano, Italy. In particular, I en-

Summary of papers

Paper I describes time-resolved measurements of the optical properties of healthy breast tissue *in vivo* and *in vitro*. Absorption and scattering properties of the tissue over a broad spectral range were determined in a single measurement. Femtosecond white light pulses were generated by self-phase modulation of high-power laser pulses focussed in water. A streak camera in combination with a spectrometer was used for time- and wavelength-resolved detection of the diffusely scattered light.

Papers II and III demonstrate the technique of reconstructing the interference between photon density waves. Interference between two waves could be reconstructed at any chosen modulation frequency from two consecutive time-resolved measurements. By having a time delay between the light pulses in the time domain, a phase shift was obtained in the frequency domain. It was demonstrated that inclusions in a tissue phantom with realistic optical properties could be detected using this technique. In Paper II the method of reversing the setup, so that a single light source and multiple detectors could be used, is demonstrated.

Papers IV and V report on frequency-resolved photon migration measurements using a broad-band system operating at several light wavelengths. In Paper IV, the optical properties of fat are determined, and the analysis routine for determination of tissue physiological properties is expanded to include fat concentration extraction. An *in vivo* case study is presented, showing that realistic concentrations of oxy- and deoxy-haemoglobin, fat and water of breast tissue can be obtained with this technique. Paper V presents more *in vivo* data from frequency-resolved photon migration measurements on healthy breast tissue. Hormonal changes due to menopausal status, menstrual cycle etc. cause large variations in water concentration and blood volume and oxygenation, which in turn affects the optical properties measured.

Papers VI and VII deal with clinical laser-induced fluorescence measurements from the colon. In Paper VI it was shown that adenomatous tissue could be distinguished from healthy tissue from fluorescence data obtained with 337 nm excitation (where no tumour marker was needed) and with 405 or 436 nm excitation in ALA patients. In Paper VII, it is shown that neoplastic polyps can be distinguished from non-neoplastic polyps using 337 nm excitation. Partial least squares analysis was used for tissue classification. 405 nm excitation in ALA patients is not successful for this purpose, indicating a poor selectivity of the substance in colonic epithelial polyps.

Papers VIII and IX present fluorescence spectral data obtained *in vivo* from the vocal and ventricular folds in the larynx. In Paper VIII fluorescence intensities and intensity ratios are used for distinguishing different degrees of neoplastic progression. Paper IX evaluates some multivariate analysis methods for spectral decomposition.

Paper X reports on a preliminary evaluation of two different modalities for fluorescence imaging; multi-colour and lifetime imaging. Images obtained *in vivo* on five basal cell carcinomas of the skin after topical application of ALA are shown. Both systems performed well and identified all lesions with the same degree of reliability.

Contributions to the papers from the author:

Experimental or clinical work for all papers.

Major parts of the data evaluation for Papers II-IV, VI, VII and IX.
Parts of the data evaluation for Papers V and VIII.

Writing of major parts of the manuscript for Papers II-IV,VI, VII, and IX.

References

1. R.C. Haskell, L.O. Svaasand, T.-T. Tsay, T.-C. Feng, M.S. McAdams and B.J. Tromberg, Boundary conditions for the diffusion equation in radiative transfer, *J. Opt. Soc. Am. A* **11**, 2727-2741 (1994).

2. M. Cutler, Transilluminating as an aid in the diagnosis of breast lesions, *Surg. Gynecol. Obstet.* **48**, 721-728 (1929).

3. A. Policard, Études sur les aspects offerts par des tumeur expérimentales examinée à la lumière de Woods, *CR. Soc. Biol.* **91**, 1423-1423 (1924).

4. N.R. Finsen, *Phototherapy*, (Edward Arnold, London, UK, 1901).

5. V.G. Peters, D.R. Wyman, M.S. Patterson and G.L. Frank, Optical properties of normal and diseased human breast tissues in the visible and near infrared, *Phys. Med. Biol.* **35**, 1317-1334 (1990).

6. T.L. Troy, D.L. Page and E.M. Sevick-Muraca, Optical properties of normal and diseased breast tissues: prognosis for optical mammography, *J. Biomedical Optics* **1**, 342-355 (1996).

7. E.N. Carlsen, Transmission spectroscopy: An improvement in light scanning, *RNM Images* **13**, 22-25 (1983).

8. H.C. Sox, Benefit and harm associated with screening for breast cancer, *N. Engl. J. Med.* **338**, 1145-1145 (1998).

9. P.J. McKinnon, Ataxia-telangiectasia: an inherited disorder of ionizing-radiation sensitivity in man. Progress in the elucidation of the underlying biochemical defect, *Hum. Genet.* **75**, 197-208 (1987).

10. A.A. Oraevsky, V.S. Letokhov, V.G. Omal'yanenko, S.E. Ragimov, A.A. Belyaev, B.V. Shekhonin and R.S. Akchurin, Laser spectral analysis of human atherosclerotic vessels, in *Laser Spectroscopy VIII,* eds. W. Persson and S. Svanberg, pp. 370-371 (Springer Verlag, Berlin, Heidelberg, Germany, 1987).

11. R. Richards-Kortum, A. Mehta, T. Kolubayev, C. Hoyt, R. Cothren, B. Sacks, C. Kittrell, M.S. Feld, N.B. Ratliff, T. Kjellstrom, G. Bordagaray, M. Fitzmaurice and J. Kramer, Spectroscopic diagnosis for control of laser treatment of atherosclerosis, in *Laser Spectroscopy VIII,* eds. W. Persson and S. Svanberg, pp. 366-369 (Springer Verlag, Berlin, Heidelberg, Germany, 1987).

12. S. Andersson-Engels, A. Gustafson, J. Johansson, U. Stenram, K. Svanberg and S. Svanberg, Laser-induced fluorescence used in localizing atherosclerotic lesions, *Lasers Med. Sci.* **4**, 171-181 (1989).

13. H. Stübel, Die Fluoreszenz tierischer Gewebe in ultravioletten Licht, *Pflügers Arch.* **142**, 1-1 (1911).

14. J.J. Baraga, P. Taroni, Y.D. Park, K. An, A. Maestri, L.L. Tong, R.P. Rava, C. Kittrell, R.R. Dasari and M.S. Feld, Ultraviolet laser induced fluorescence of human aorta, *Spectrochim. Acta* **45A**, 95-99 (1989).

15. B. Chance, P. Cohen, F. Jöbsis and B. Schoener, Intracellular oxidation-reduction states in vivo, *Science* **137**, 499-508 (1962).

16. B. Chance and B. Schoener, Fluorometric studies of flavin component of respiratory chain, in *Flavins and flavoproteins,* ed. Slater, pp. 510-519 (Elsevier Publishing Comp, New York, USA, 1966).

17. A.E. Profio, D.R. Doiron, O.J. Balchum and G.C. Huth, Fluorescence bronchoscopy for localization of carcinoma *in situ*, *Med. Phys.* **10**, 35-39 (1983).

18. R.R. Alfano, D.B. Tata, J. Cordero, P. Tomashefsky, F.W. Longo and M.A. Alfano, Laser induced fluorescence spectroscopy from native cancerous and normal tissue, *IEEE J. Quant. Electr.* **QE-20**, 1507-1511 (1984).

19. P.S. Andersson, E. Kjellén, S. Montán, K. Svanberg and S. Svanberg, Autofluorescence of various rodent tissues and human skin tumour samples, *Lasers Med. Sci.* **2**, 41-49 (1987).

20. D.S. Rasmussen-Taxdal, G.E. Ward and F.H.J. Figge, Fluorescence of human lymphatic and cancer tissues following high doses of intraveneous haematoporphyrin, *Cancer* **8**, 78-81 (1955).

21. H.B. Gregorie and J.F. Green, Haematoporphyrin derivative fluorescence in malignant neoplasms, *J. S. C. Med. Assoc.* **61**, 157-164 (1965).

22. I.J. Bigio and J.R. Mourant, Ultraviolet and visible spectroscopies for tissue diagnostics: fluorescence spectroscopy and elastic-scattering spectroscopy, *Phys. Med. Biol.* **42**, 803-814 (1997).

23. S. Andersson-Engels, J. Johansson, K. Svanberg and S. Svanberg, Fluorescence imaging and point measurements of tissue: Applications to the demarcation of malignant tumors and atherosclerotic lesions from normal tissue, *Photochem. Photobiol.* **53**, 807-814 (1991).

24. A. Ishimaru, *Wave Propagation and Scattering in Random Media*, (Academic Press, New York, NY, 1978).

25. L.G. Henyey and J.L. Greenstein, Diffuse radiation in the galaxy, *Astrophys. J.* **93**, 70-83 (1941).

26. K.M. Case and P.F. Zweifel, *Linear Transport Theory*, (Addison-Wesley Publishing Co., Reading, MA, 1967).

27. K. Furutsu and Y. Yamada, Diffusion approximation for a dissipative random medium and the applications, *Phys. Rev. E* **50**, 3634-3640 (1994).

28. H.C. van de Hulst and R. Graaff, Aspects of similarity in tissue optics with strong forward scattering, *Phys. Med. Biol.* **41**, 2519-2531 (1996).

29. M.S. Patterson, B. Chance and B.C. Wilson, Time resolved reflectance and transmittance for the non-invasive measurement of optical properties, *Appl. Opt.* **28**, 2331-2336 (1989).

30. T.J. Farrell, M.S. Patterson and B. Wilson, A diffusion theory model of spatially resolved, steady-state diffuse reflectance for noninvasive determination of tissue optical properties *in vivo*, *Med. Phys.* **19**, 879-888 (1992).

31. M. Keijzer, W.M. Star and P.R.M. Storchi, Optical diffusion in layered media, *Appl. Opt.* **27**, 1820-1824 (1988).

32. J.B. Fishkin and E. Gratton, Propagation of photon-density waves in strongly scattering media containing an absorbing semiinfinite plane bounded by a straight edge, *J. Opt. Soc. Am. A* **10**, 127-140 (1993).

33. B.C. Wilson, Measurements of tissue optical properties: Methods and theories, in *Optical-Thermal Response of Laser-Irradiated Tissue,* eds. A.J. Welch and M.J.C. van Gemert, pp. 233-274 (Plenum Press, New York, 1995).

34. R.A.J. Groenhuis, H.A. Ferwerda and J.J. ten Bosch, Scattering and absorption of turbid materials determined from reflection measurements. 1: Theory, *Appl. Opt.* **22**, 2456-2462 (1983).

35. J.-L. Boulnois, Photophysical processes in recent medical laser developments: a review, *Lasers Med. Sci.* **1**, 47-66 (1986).

36. F.A. Duck, *Physical Properties of Tissue*, (Academic Press Ltd., London, 1990).

37. G.M. Hale and M.R. Querry, Optical constants of water in the 200-nm to 200-μm wavelength region, *Appl. Opt.* **12**, 555-563 (1973).

38. S.A. Prahl, Tabulated molar extinction coefficient for hemoglobin in water, http://omlc.ogi.edu/spectra/hemoglobin/summary.html, (1998).

39. J.S. Wyatt, M. Cope, D.T. Delpy, S. Wray and E.O.R. Reynolds, Quantification of cerebral oxygenation and haemodynamics in sick newborn infants by near infrared spectrophotometry, *Lancet* 1063-1066 (1986).

40. M. Cope and D.T. Delpy, System for long-term measurement of cerebral blood and tissue oxygenation on newborn infants by near infra-red transillumination, *Med. Biol. Eng. Comput.* **26**, 289-294 (1988).

41. B. Chance, Near-infrared images using continuous, phase-modulated, and pulsed light with quantitation of blood and blood oxygenation., *Ann. N. Y. Acad. Sci.* **838**, 29-45 (1998).

42. T. Spott, Characterization of layered tissue structures with diffusely propagating photon-density waves, Dissertation thesis, Norweigan University of Science and Technology, Department of Physical Electronics, Trondheim, Norway, (1999).

43. H.Q. Woodard and D.R. White, The composition of body tissues, *Br. J. Radiol.* **59**, 1209-1218 (1986).

44. S.L. Jacques and D.J. McAuliffe, The melanosome: Threshold temperature for explosive vaporization and internal absorption coefficient during pulsed laser irradiation, *Photochem. Photobiol.* **53**, 769-775 (1991).

45. W.-F. Cheong, Summary of optical properties, in *Optical-Thermal Response of Laser-Irradiated Tissue,* eds. A.J. Welch and M.J.C. van Gemert, pp. 275-303 (Plenum Press, New York, 1995).

46. F.P. Bolin, L.E. Preuss, R.C. Taylor and R.J. Ference, Refractive index of some mammalian tissue using a fiber optic cladding method, *Appl. Opt.* **28**, 2297-2303 (1989).

47. G.J. Tearney, M.E. Brezinski, J.F. Southern, B.E. Bouma, M.R. Hee and J.G. Fujimoto, Detrmination of the refractive index of highly scattering human tissue by optical coherence tomography, *Opt. Lett.* **20**, 2258-2260 (1995).

48. J. Beuthan, O. Minet, J. Helfmann, M. Herrig and G. Müller, The spatial variation of the refractive index in biological cells, *Phys. Med. Biol.* **41**, 369-382 (1996).

49. B. Beauvoit, S.M. Evans, T.W. Jenkins, E.E. Miller and B. Chance, Correlation between the light scattering and the mitochondrial content of normal tissues and transplantable rodent tumors, *Anal. Biochem.* **226**, 167-174 (1995).

50. P. Latimer, D.M. Moore and F. Dudley Bryant, Changes in total light scattering and absorption caused by changes in particle conformation, *J. Theor. Biol.* **21**, 348-367 (1968).

51. J.R. Mourant, J.P. Freyer, A.H. Hielscher, A.A. Eick, D. Shen and T.M. Johnson, Mechanisms of light scattering from biological cells relevant to noninvasive optical-tissue diagnotics, *Appl. Opt.* **37**, 3586-3593 (1998).

52. A.M.K. Nilsson, C. Sturesson, D.L. Liu and S. Andersson-Engels, Changes in spectral shape of tissue optical properties in conjunction with laser-induced thermotherapy, *Appl. Opt.* **37**, 1256-1267 (1998).

53. I.S. Saidi, S.L. Jacques and F.K. Tittel, Mie and Rayleigh modeling of visible-light scattering in neonatal skin, *Appl. Opt.* **34**, 7410-7418 (1995).

54. T. Kitai, B. Beauvoit and B. Chance, Optical determination of fatty change of the graft liver with near-infrared time-resolved spectroscopy, *Transplantation* **62**, 642-647 (1996).

55. J.W. Pickering, S.A. Prahl, N. van Wieringen, J.F. Beek, H.J.C.M. Sterenborg and M.J.C. van Gemert, Double-integrating-sphere system for measuring the optical properties of tissue, *Appl. Opt.* **32**, 399-410 (1993).

56. M.S. Patterson, J.D. Moulton, B.C. Wilson, K.W. Berndt and J.R. Lakowicz, Frequency-domain reflectance for the determination of the scattering and absorption properties of tissue, *Appl. Opt.* **30**, 4474-4476 (1991).

57. G.J. Müller, B. Chance, R.R. Alfano, S.R. Arridge, J. Beuthan, E. Gratton, M. Kaschke, B.R. Masters, S. Svanberg and P. van der Zee, eds., *Medical optical tomography: Functional imaging and monitoring*, SPIE Institute Series, vol. **11**, (SPIE Optical Engineering Press, Bellingham, WA, 1993).

58. L. Garfinkel, Cancer statistics and trends, in *American Cancer Society Textbook of Clinical Oncology,* eds. A.I. Holleb, D.J. Fink and G.P. Murphy, pp. 1-6 (American Cancer Society, Atlanta, GA, 1991).

59. S.A. Bartow, The breast, in *Pathology,* eds. E. Rubin and J.L. Farber, pp. 973-992 (J.B. Lippincott, Philadelphia, 1994).

60. S. Thomsen and D. Tatman, Physiological and pathological factors of human breast disease that can influence optical diagnosis, *Ann. N. Y. Acad. Sci.* **838**, 171-193 (1998).

61. M. Swift, D. Morell, R.B. Massey and C.L. Chase, Incidence of cancer in 161 families affected by ataxia-telangiectasia, *N. Engl. J. Med.* **325**, 1831-1836 (1991).

62. R. Berg, S. Andersson-Engels, O. Jarlman and S. Svanberg, Time-gated viewing studies on tissuelike phantoms, *Appl. Opt.* **35**, 3432-3440 (1996).

63. S.T. Flock, S.L. Jacques, B.C. Wilson, W.M. Star and M.J.C. van Gemert, Optical properties of Intralipid: A phantom medium for light propagation studies, *Lasers Surg. Med.* **12**, 510-519 (1992).

64. S.J. Madsen, M.S. Patterson and B.C. Wilson, The use of india ink as an optical absorber in tissue-simulating phantoms, *Phys. Med. Biol.* **37**, 985-993 (1992).

65. R. Cubeddu, A. Pifferi, P. Taroni, A. Torricelli and G. Valentini, A solid tissue phantom for photon migration studies, *Phys. Med. Biol.* **42**, 1971-1979 (1997).

66. M. Firbank, M. Oda and D.T. Delpy, An improved design for a stable and reproducable phantom material for use in near-infrared spectroscopy and imaging, *Phys. Med. Biol.* **40**, 955-961 (1995).

67. U. Sukowski, F. Schubert, D. Grosenick and H. Rinneberg, Preparation of solid phantoms with defined scattering and absorption properties for optical tomography, *Phys. Med. Biol.* **41**, 1823-1844 (1996).

68. J.C. Hebden, R.A. Kruger and K.S. Wong, Time resolved imaging through a highly scattering medium, *Appl. Opt.* **30**, 788-794 (1991).

69. S. Andersson-Engels, R. Berg, O. Jarlman and S. Svanberg, Time-resolved transillumination for medical diagnostics, *Opt. Lett.* **15**, 1179-1181 (1990).

70. S. Andersson-Engels, R. Berg and S. Svanberg, Effects of optical constants on time-gated transillumination of tissue and tissue-like media, *J. Photochem. Photobiol. B* **16**, 155-167 (1992).

71. R. Berg, O. Jarlman and S. Svanberg, Medical transillumination imaging using short-pulse diode lasers, *Appl. Opt.* **32**, 574-579 (1993).

72. S. Andersson-Engels, R. Berg, A. Persson and S. Svanberg, Multispectral tissue characterization with time-resolved detection of diffusely scattered white light, *Opt. Lett.* **18**, 1697-1699 (1993).

73. R.W. Boyd, *Nonlinear Optics*, (Academic Press, Inc., San Diego, CA, 1992).

74. J.M. Schmitt, A. Knüttel and J.R. Knutson, Interference of diffusive lightwaves, *J. Opt. Soc. Am.* **9**, 1832-1843 (1992).

75. A. Knüttel, J.M. Schmitt and J.R. Knutson, Spatial localization of absorbing bodies by interfering diffusive photon-density waves, *Appl. Opt.* **32**, 381-389 (1993).

76. B. Chance, K. Kang, L. He, J. Weng and E. Sevick, Highly sensitive object location in tissue models with linear in-phase and anti-phase multi-element optical arrays in one and two dimensions, *Proc. Natl. Acad. Sci. USA* **90**, 3423-3427 (1995).

77. M.A. O'Leary, D.A. Boas, B. Chance and A.G. Yodh, Experimental images of heterogeneous turbid media by frequency- domain diffusing-photon tomography, *Opt. Lett.* **20**, 426-428 (1995).

78. B.J. Tromberg, L.O. Svaasand, T.-T. Tsay and R.C. Haskell, Properties of photon density waves in multiple-scattering media, *Appl. Opt.* **32**, 607-616 (1993).

79. E.M. Sevick, J.K. Frisoli, C.L. Burch and J.R. Lakowicz, Localization of absorbers in scattering media by use of frequency-domain measurements of time-dependent photon migration, *Appl. Opt.* **33**, 3562-3570 (1994).

80. S.J. Madsen, E.R. Anderson, R.C. Haskell and B.J. Tromberg, Portable, high-bandwidth frequency-domain photon migration instrument for tissue spectroscopy, *Opt. Lett.* **19**, 1934-1936 (1994).

81. K.P. Chan, M. Yamada, B. Devaraj and H. Inaba, Optical imaging through highly scattering media by use of heterodyne detection in the 1.3-μm wavelength region, *Opt. Lett.* **20**, 492-494 (1995).

82. E. Gratton, W.W. Mantulin, M.J. vandeVen, J. Fishkin, M.B. Maris and B. Chance, A novel approach to laser tomography, *Bioimaging* **1**, 40-46 (1993).

83. S. Fantini, M.A. Franceschini-Fantini, J.S. Maier, S.A. Walker, B. Barbieri and E. Gratton, Frequency-domain multichannel optical

detector for noninvasive tissue spectroscopy and oximetry, *Opt. Eng.* **34**, 32-42 (1995).

84. E.M. Sevick, B. Chance, J. Leigh, S. Nioka and M. Maris, Quantitation of time- and frequency-resolved optical spectra for determination of tissue oxygenation, *Anal. Biochem.* **195**, 330-351 (1991).

85. R. Cubeddu, A. Pifferi, P. Taroni, A. Torricelli and G. Valentini, Compact tissue oximeter based on dual-wavelength multichannel time-resolved reflectance, *Appl. Opt.* **38**, 3670-3680 (1999).

86. B.C. Wilson, E.M. Sevick, M.S. Patterson and B. Chance, Time-dependent optical spectroscopy and imaging for biomedical applications, *Proc. IEEE* **80**, 918-930 (1992).

87. J.B. Fishkin, O. Coquoz, E.R. Anderson, M. Brenner and B.J. Tromberg, Frequency-domain photon migration measurements of normal and malignant tissue optical properties in a human subject, *Appl. Opt.* **36**, 10-20 (1997).

88. B.J. Tromberg, O. Coquoz, J.B. Fishkin, T. Pham, E.R. Anderson, J. Butler, M. Cahn, J.D. Gross, V. Venugopalan and D. Pham, Noninvasive measurements of breast tissue optical properties using frequency-domain photon migration, *Phil. Trans. R. Soc. Lond. B* **352**, 661-668 (1997).

89. R. Cubeddu, A. Pifferi, P. Taroni, A. Torricelli and G. Valentini, Noninvasive absorption and scattering spectroscopy of bulk diffusive media: An application to the optical characterization of human breast, *Appl. Phys. Lett.* **74**, 874-876 (1999).

90. V. Quaresima, S.J. Matcher and M. Ferrari, Identification and quantification of intrinsic optical contrast for near-infrared mammography, *Photochem. Photobiol.* **67**, 4-14 (1998).

91. S. Andersson-Engels and B.C. Wilson, *In vivo* fluorescence in clinical oncology: Fundamental and practical issues, *J. Cell Pharmacol.* **3**, 48-61 (1992).

92. B. Palcic, S. Lam, J. Hung and C. MacAulay, Detection and localization of early lung cancer by imaging techniques, *Chest* **99**, 742-743 (1991).

93. R.Y. Demers, A.V. Neale, H. Budev and W.J. Schade, Pathologist agreement in the interpretation of colorectal polyps, *Am. J. Gastroenterol.* **85**, 417-421 (1990).

94. K.T. Schomacker, J.K. Frisoli, C.C. Compton, T.J. Flotte, J.M. Richter, N.S. Nishioka and T.F. Deutsch, Ultraviolet laser-induced fluorescence of colonic tissue: Basic biology and diagnostic potential, *Lasers Surg. Med.* **12**, 63-78 (1992).

95. D.J. Fink, Cancer detction: The cancer-related checkup guidelines, in *American Cancer Society Textbook of Clinical Oncology,* eds. A.I. Holleb, D.J. Fink and G.P. Murphy, pp. 153-176 (American Cancer Society, Atlanta, GA, 1991).

96. A.V. Neale, R.Y. Demers, H. Budev and R.O. Scott, Physician accuracy in diagnosing colorectal polyps, *Dis. Col. & Rect.* **30**, 247-250 (1987).

97. M. Andreasson and O. Sandström, The design and implementation of a compact fluorosensor for medical diagnostics, Master's thesis, Lund Institute of Technology, Lund, Sweden, **LRAP-239**(1998).

98. C. af Klinteberg, M. Andreasson, O. Sandström, S. Andersson-Engels and S. Svanberg, Compact medical fluorosensor for minimally invasive tissue characterisation, Manuscript in preparation (1999).

99. C.M. Norris Jr. and B. Cady, Head, neck, and thyroid cancer, in *American Cancer Society Textbook of Clinical Oncology,* eds. A.I. Holleb, D.J. Fink and G.P. Murphy, pp. 306-328 (American Cancer Society, Atlanta, GA, 1991).

100. D.D. DeWeese, W.H. Saunders, D.E. Schuller and A.J. Schleuning II, *Otolaryngology -head and neck surgery*, (C.V.Mosby Company, St. Louis, 1988).

101. A. Mahadevan, M.F. Mitchell, E. Silva, S. Thomsen and R. Richards-Kortum, Study of the fluorescence properties of normal and neoplastic human cervical tissue, *Lasers Surg. Med.* **13**, 647-655 (1993).

102. R. Richards-Kortum, R.P. Rava, R.E. Petras, M. Fitzmaurice, M. Sivak and M.S. Feld, Spectroscopic diagnosis of colonic dysplasia, *Photochem. Photobiol.* **53**, 777-786 (1991).

103. H.J.C.M. Sterenborg, M. Motamedi, R.F. Wagner, M.L. Duvic, S. Thomsen and S.L. Jacques, In vivo fluorescence spectroscopy and imaging of human skin tumors, *Lasers Med. Sci.* **9**, 191-201 (1994).

104. R. Cubeddu, G. Canti, P. Taroni and G. Valentini, Time-gated fluorescence imaging for the diagnosis of tumors in a murine model, *Photochem. Photobiol.* **57**, 480-485 (1993).

105. S. Andersson-Engels, J. Johansson, U. Stenram, K. Svanberg and S. Svanberg, Time-resolved laser-induced fluorescence spectroscopy for enhanced demarcation of human atherosclerotic plaques, *J. Photochem. Photobiol. B* **4**, 363-369 (1990).

106. R.R. Alfano, G.C. Tang, A. Pradhan, M. Bleich, D.S.J. Choy and E. Opher, Steady state and time-resolved laser fluorescence from normal and tumor lung and breast tissues, *J. Tumor Mark. Onc.* **3**, 165-174 (1988).

107. S. Andersson-Engels, L. Baert, R. Berg, M.A. D'Hallewin, J. Johansson, U. Stenram, K. Svanberg and S. Svanberg, Fluorescence characteristics of human atherosclerotic plaque and malignant tumors, in *Optical Methods for Tumor Treatment and Early Diagnosis: Mechanisms and Techniques*, ed. T.J. Dougherty, Proc. SPIE vol. **1426**, 31-43 (1991).

108. J. Johansson, Fluorescence spectroscopy for medical and environmental diagnostics, Dissertation thesis, Lund Institute of Technology, Lund, Sweden, (1993).

109. B. Alberts, D. Bray, J. Lewis, M. Raff, K. Roberts and J.D. Watson, *Molecular Biology of the Cell*, (Garland Publishing Inc., New York, USA, 1994).

110. R.P. Rava, R. Richards-Kortum, M. Fitzmaurice, R. Cothren, R. Petras, M. Sivak, H. Levin and M.S. Feld, Early detection of dysplasia in colon and bladder tissue using laser induced fluorescence, in *Optical Methods for Tumor Treatment and Early Diagnosis: Mechanisms and Techniques*, ed. T.J. Dougherty, Proc. SPIE vol. **1426**, 68-78 (1991).

111. B. Chance, Pyridine nucleotide as an indicator of the oxygen requirements for energy-linked functions of mitochondria, *Circ. Res.* **38**, I-31-I-38 (1976).

112. B. Chance and B. Schoener, Correlation of oxidation-reduction changes of intracellular reduced pyridine nucleotide and changes in electroencephalogram of the rat in anoxia, *Nature* **195**, 956-958 (1962).

113. R.C. Benson, R.A. Meyer, M.E. Zaruba and G.M. McKhann, Cellular autofluorescence - is it due to flavins?, *J. Histochem. Cytochem.* **27**, 44-48 (1979).

114. M. Tsuchida, T. Miura and K. Aibara, Lipofuscin and lipofuscin-like substances, *Chemistry and Physics of Lipids* **44**, 297-325 (1987).

115. Y. Yang, Y. Ye, F. Li, Y. Li and P. Ma, Characteristic autofluorescence for cancer diagnosis and its origin, *Lasers Surg. Med.* **7**, 528-532 (1987).

116. L. Baert, R. Berg, B. van Damme, M.A. D'Hallewin, J. Johansson, K. Svanberg and S. Svanberg, Clinical fluorescence diagnosis of human bladder carcinoma following low-dose Photofrin injection, *Urology* **41**, 322-330 (1993).

117. C.R. Kapadia, F.W. Cutruzzola, K.M. O'Brien, M.L. Stetz, R. Enriquez and L.I. Deckelbaum, Laser-induced fluorescence spectroscopy of human colonic mucosa: Detection of adenomatous transformation, *Gastroenterology* **99**, 150-157 (1990).

118. S. Andersson-Engels, Å. Elner, J. Johansson, S.-E. Karlsson, L.G. Salford, L.-G. Strömblad, K. Svanberg and S. Svanberg, Clinical recording of laser-induced fluorescence spectra for evaluation of tumour demarcation feasibility in selected clinical specialities, *Lasers Med. Sci.* **6**, 415-424 (1991).

119. G. Zonios, R. Cothren, J.M. Crawford, M. Fitzmaurice, R. Manoharan, J. van Dam and M.S. Feld, Spectral pathology, *Ann. N. Y. Acad. Sci.* **838**, 108-115 (1998).

120. T.J. Römer, M. Fitzmaurice, R.M. Cothren, R. Richards-Kortum, R. Petras, M.V. Sivak and J.R. Kramer, Laser-induced fluorescence microscopy of normal colon and dysplasia in colonic adenomas: Impli-

cations for spectroscopic diagnosis, *Am. J. Gastroenterol.* **90**, 81-87 (1995).

121. G.S. Fiarman, M.H. Nathanson, A.B. West, L.I. Deckelbaum, L. Kelly and C.R. Kapadia, Differences in laser-induced autofluorescence between adenomatous and hyperplastic polyps and normal colonic mucosa by confocal microscopy, *Dig. Dis. Sci.* **40**, 1261-1268 (1995).

122. R.S. DaCosta, H. Andersson, B.C. Wilson, M. Cirocco, S. Hassaram and N.E. Marcon, Correlative studies of autofluorescence, immuno/histopathology and ultrastructures of ex vivo tissues and primary cultured epithelial cells from human normal, preneoplastic and neoplastic colorectal mucosa, *CLEO/Europe - EQEC Focus Meetings*, München, Germany, 6-13-1999.

123. R. Bonnett and M. Berenbaum, Porphyrins as photosensitizers, in *Photosensitizing Compounds: their Chemistry, Biology and Clinical Use,* eds. G. Bock and S. Harnett, pp. 40-59 (John Wiley & Sons Ltd, Chichester, UK, 1989).

124. J.C. Kennedy and R.H. Pottier, Endogenous protoporphyrin IX, a clinically useful photosensitizer for photodynamic therapy, *J. Photochem. Photobiol. B* **14**, 275-292 (1992).

125. C.S. Loh, A.J. MacRobert, J. Bedwell, J. Regula, N. Krasner and S.G. Bown, Oral versus intravenous administration of 5-aminolevulinic acid for photodynamic therapy, *Br. J. Cancer* **68**, 41-51 (1993).

126. Q. Peng, J.F. Evensen, C. Rimington and J. Moan, A comparison of different photosensitizing dyes with respect to uptake C3H-tumors and tissues of mice, *Cancer Lett.* **36**, 1-10 (1987).

127. N. Schoenfeld, O. Epstein, M. Lahav, R. Mamet, M. Shaklai and A. Atsmon, The heme biosynthetic pathway in lymphocytes of patients with malignant lymphoproliferative disorders, *Cancer Lett.* **43**, 43-48 (1988).

128. A. Jarrett, C. Rimington and D.A. Willoughby, δ-aminolaevulic acid and porphyria, *Lancet* 125-127 (1956).

129. N.I. Berlin, A. Neuberger and J.J. Scott, The metabolism of δ-aminolaevulic acid. 2. Normal pathways, studied with the aid of ¹⁴C, *Biochem. J.* **64**, 90-100 (1956).

130. J.C. Kennedy, R.H. Pottier and D.C. Pross, Photodynamic therapy with endogenous protoporphyrin IX: Basic principles and present clinical experience, *J. Photochem. Photobiol. B* **6**, 143-148 (1990).

131. K. Svanberg, T. Andersson, D. Killander, I. Wang, U. Stenram, S. Andersson-Engels, R. Berg, J. Johansson and S. Svanberg, Photodynamic therapy of non-melanoma malignant tumours of the skin using topical δ-amino levulinic acid sensitization and laser irradiation, *Br. J. Dermatol.* **130**, 743-751 (1994).

132. H. Heyerdahl, I. Wang, D.L. Liu, R. Berg, S. Andersson-Engels, Q. Peng, J. Moan, S. Svanberg and K. Svanberg, Pharmacokinetic studies on 5-aminolevulinic acid-induced protoporphyrin IX accumulation in tumours and normal tissues, *Cancer Lett.* **112**, 225-231 (1997).

133. I. Wang, L. Pais Clemente, R.M.G. Pratas, E. Cardoso, M. Pais Clemente, S. Montán, S. Svanberg and K. Svanberg, Fluorescence diagnostics and kinetic studies in the head and neck region utilizing low-dose δ-aminolevulinic acid sensitization, *Cancer Lett.* **135**, 11-19 (1999).

134. C. af Klinteberg, A.M.K. Nilsson, I. Wang, S. Andersson-Engels, S. Svanberg and K. Svanberg, Laser-induced fluorescence diagnostics of basal cell carcinomas of the skin following topical ALA application, in *Optical Biopsies and Microscopic Techniques*, eds. I.J. Bigio, W.S. Grundfest, H. Schneckenburger, K. Svanberg and P.M. Viallet, Proc. SPIE vol. **2926**, 32-40 (1996).

135. S. Montán, K. Svanberg and S. Svanberg, Multi-color imaging and contrast enhancement in cancer tumor localization using laser-induced fluorescence in hematoporphyrin derivative (HpD)-bearing tissue, *Opt. Lett.* **10**, 56-58 (1985).

136. P.S. Andersson, S. Montán and S. Svanberg, Multi-spectral system for medical fluorescence imaging, *IEEE J. Quant. Electr.* **QE-23**, 1798-1805 (1987).

137. S. Andersson-Engels, J. Johansson and S. Svanberg, Medical diagnostic system based on simultaneous multispectral fluorescence imaging, *Appl. Opt.* **33**, 8022-8029 (1994).

138. K. Svanberg, I. Wang, S. Colleen, I. Idvall, C. Ingvar, R. Rydell, D. Jocham, H. Diddens, S. Bown, G. Gregory, S. Montán, S. Andersson-Engels and S. Svanberg, Clinical multi-colour fluorescence imaging of malignant tumours - initial experience, *Acta Radiol.* **39**, 2-9 (1998).

139. R. Baumgartner, H. Fisslinger, D. Jocham, H. Lenz, L. Ruprecht, H. Stepp and E. Unsöld, A fluorescence imaging device for endoscopic detection of early stage cancer - instrumental and experimental studies, *Photochem. Photobiol.* **46**, 759-763 (1987).

140. M. Keijzer, R.R. Richards-Kortum, S.L. Jacques and M.S. Feld, Fluorescence spectroscopy of turbid media: Autofluorescence of the human aorta, *Appl. Opt.* **28**, 4286-4292 (1989).

141. S. Andersson-Engels, J. Johansson and S. Svanberg, The use of time-resolved fluorescence for diagnosis of atherosclerotic plaque and malignant tumours, *Spectrochim. Acta* **46A**, 1203-1210 (1990).

142. R. Cubeddu, P. Taroni and G. Valentini, Time-gated imaging system for tumor diagnosis, *Opt. Eng.* **32**, 320-325 (1993).

143. Q. Peng, T. Warloe, K. Berg, J. Moan, M. Kongshaug, K.-E. Giercksky and J.M. Nesland, 5-aminolevulinic acid-based photodynamic therapy: Clinical research and future challenges, *Cancer* **79**, 2282-2308 (1997).

144. K. Svanberg, D.L. Liu, I. Wang, S. Andersson-Engels, U. Stenram and S. Svanberg, Photodynamic therapy using intravenous δ-aminolaevulinic acid-induced protoporphyrin IX sensitisation in experimental hepatic tumours in rats, *Br. J. Cancer* **74**, 1526-1533 (1996).

145. T. Andersson, R. Berg, J. Johansson, D. Killander, K. Svanberg, S. Svanberg and Y.L. Yang, Photodynamic therapy in interplay with fluorescence diagnostics in the treatment of human superficial malignancies, in *Optical Methods for Tumor Treatment and Detection: Mecha-*

nisms and Techniques in Photodynamic Therapy, ed. T.J. Dougherty, Proc. SPIE vol. **1645**, 187-199 (1992).

146. M.A. D'Hallewin and L. Baert, Long-term results of whole bladder wall photodynamic therapy for carcinoma in situ of the bladder, *Urology* **45**, 763-767 (1995).

147. C.P. Lowdell, D.V. Ash, I. Driver and S.B. Brown, Interstitial photodynamic therapy. Clinical experience with diffusing fibres in the treatment of cutaneous and subcutaneous tumours, *Br. J. Cancer* **67**, 1398-1403 (1993).

148. N. Ohlsson and O. Rylow, Development of a multifibre system for interstitial photodynamic therapy of malignant tumours, Master's thesis, Lund Institute of Technology, Lund, Sweden, **LRAP-240** (1998).

149. N. Ramanujam, M.F. Mitchell, A. Mahadevan, S. Thomsen, E. Silva and R. Richards-Kortum, Fluorescence spectroscopy: a diagnostic tool for cervical intraepithelial neoplasia (CIN), *Gynecol. Oncol.* **52**, 31-38 (1994).

150. R. Richards-Kortum, Fluorescence spectroscopy of turbid media, in *Optical-Thermal Response of Laser-Irradiated Tissue,* eds. A.J. Welch and M.J.C. van Gemert, pp. 667-707 (Plenum Press, New York, 1995).

151. N. Ramanujam, M.F. Mitchell, A. Mahadevan, S. Warren, S. Thomsen, E. Silva and R. Richards-Kortum, *In vivo* diagnosis of cervical intraepithelial neoplasia using 337-nm-excited laser-induced fluorescence, *Proc. Natl. Acad. Sci. USA* **91**, 10193-10197 (1994).

152. R. Richards-Kortum, R.P. Rava, M. Fitzmaurice, L.L. Tong, N.B. Ratliff, J.R. Kramer and M.S. Feld, A one-layer model of laser-induced fluorescence for diagnosis of disease in human tissue: applications to atherosclerosis, *IEEE Trans. Biomed. Eng.* **36**, 1222-1232 (1989).

153. C. af Klinteberg, I. Wang, A.M.K. Enejder, S. Andersson-Engels, S. Svanberg and K. Svanberg, 5-Aminolevulinic acid-induced protoporphyrin IX fluorescence in basal cell carcinomas of the skin, Submitted to Photochem. Photobiol. (1999).

154. H. Martens and T. Naes, *Multivariate Calibration*, (Wiley & Sons Ltd, 1991).

155. K. Esbensen, S. Schönkopf, T. Midtgaard and D. Guyot, *Multivariate Analysis in Practice*, (CAMO ASA, Norway, 1998).

156. N. Ramanujam, M.F. Mitchell, A. Mahadevan-Jensen, S.L. Thomsen, G. Staerkel, A. Malpica, T. Wright, N. Atkinson and R. Richards-Kortum, Cervical precancer detection using a multivariate statistical algorithm based on laser-induced fluorescence spectra at multiple excitation wavelengths, *Photochem. Photobiol.* **64**, 720-735 (1996).

157. K.M. O'Brien, A.F. Gmitro, G.R. Gindi, M.L. Stetz, F.W. Cutruzzola, L.I. Laifer and L.I. Deckelbaum, Development and evaluation of spectral classification algorithms for fluorescence guided laser angioplasty, *IEEE Trans. Biomed. Eng.* **36**, 424-430 (1989).

158. K.T. Schomacker, J.K. Frisoli, C.C. Compton, T.J. Flotte, J.M. Richter, T.F. Deutsch and N.S. Nishioka, Ultraviolet laser-induced fluorescence of colonic polyps, *Gastroenterology* **102**, 1155-1160 (1992).

159. R. Marchesini, M. Brambilla, E. Pignoli, G. Bottiroli, A.C. Croce, M. Dal Fante, P. Spinelli and S. Di Palma, Light-induced fluorescence spectroscopy of adenomas, adenocarcinomas and non-neoplastic mucosa in human colon. I. In vitro measurements, *J. Photochem. Photobiol. B* **14**, 219-230 (1992).

160. N. Ramanujam, M.F. Mitchell, A. Mahadevan, S. Thomsen, A. Malpica, T. Wright, N. Atkinson and R. Richards-Kortum, Development of a multivariate statistical algorithm to analyze human cervical tissue fluorescence spectra acquired in vivo, *Lasers Surg. Med.* **19**, 46-62 (1996).

161. E.B. Hanlon, I. Itzkan, R.R. Dasari, M.S. Feld, R.J. Ferrante, A.C. McKee, D. Lathi and N.W. Kowall, Near-infrared fluorescence spectroscopy detects Alzheimer's disease *in vitro*, *Photochem. Photobiol.* **70**, 236-242 (1999).

162. S. Andersson-Engels, J. Johansson, U. Stenram, K. Svanberg and S. Svanberg, Malignant tumor and atherosclerotic plaque diagnosis us-

ing laser-induced fluorescence, *IEEE J. Quant. Electr.* **26**, 2207-2217 (1990).

163. D.F. Morrison, *Multivariate Statistical Methods*, (McGraw-Hill Book Company, New York, NY, 1976).

164. D.M. Haaland, H.D.T. Jones and E.V. Thomas, Multivariate classification of the infrared spectra of cell and tissue samples, *Appl. Spectr.* **51**, 340-345 (1997).

165. C.-Y. Wang, C.-T. Chen, C.-P. Chiang, S.-T. Young, S.-N. Chow and H.K. Chiang, A probability-based multivariate statistical algorithm for autofluorescence spectroscopic identification of oral carcinogenesis, *Photochem. Photobiol.* **69**, 471-477 (1999).

166. G.R. Gindi, C.J. Darken, K.M. O'Brien, M.L. Stetz and L.I. Deckelbaum, Neural network and conventional classifiers for fluorescence-guided laser angioplasty, *IEEE Trans. Biomed. Eng.* **38**, 246-252 (1991).